AWARD NUMBER: W81XWH-15-1-0070

TITLE: Development of Less Toxic Treatment Strategies for Metastatic and Drug-Resistant Breast Cancer Using Noninvasive Optical Monitoring

PRINCIPAL INVESTIGATOR: Darren Roblyer

CONTRACTING ORGANIZATION:
Boston University
Boston, MA 02215

REPORT DATE: September 2017

TYPE OF REPORT: Annual

PREPARED FOR: U.S. Army Medical Research and Materiel Command
Fort Detrick, Maryland 21702-5012

REPORT DOCUMENTATION PAGE

Form Approved
OMB No. 0704-0188

1. REPORT DATE	2. REPORT TYPE	3. DATES COVERED
September 2017	Annual	01 Sept 2016 -31 Aug 2017

4. TITLE AND SUBTITLE

Development of Less Toxic Treatment Strategies for Metastatic and Drug-Resistant Breast Cancer Using Noninvasive Optical Monitoring

5a. CONTRACT NUMBER

5b. GRANT NUMBER
W81XWH-15-1-0070

5c. PROGRAM ELEMENT NUMBER

6. AUTHOR(S)

Darren Roblyer

E-Mail:roblyer@bu.edu

5d. PROJECT NUMBER

5e. TASK NUMBER

5f. WORK UNIT NUMBER

7. PERFORMING ORGANIZATION NAME(S) AND ADDRESS(ES)

BOSTON UNIVERSITY
BOSTON MA 02215-1703

8. PERFORMING ORGANIZATION REPORT NUMBER

9. SPONSORING / MONITORING AGENCY NAME(S) AND ADDRESS(ES)

U.S. Army Medical Research and Materiel Command
Fort Detrick, Maryland 21702-5012

10. SPONSOR/MONITOR'S ACRONYM(S)

11. SPONSOR/MONITOR'S REPORT NUMBER(S)

12. DISTRIBUTION / AVAILABILITY STATEMENT

Approved for Public Release; Distribution Unlimited

13. SUPPLEMENTARY NOTES

14. ABSTRACT

This project involves the development of optically guided multi-agent therapies for metastatic and drug resistant breast cancer. Non-invasive Diffuse Optical Imaging technologies are able to monitor drug response and resistance through quantitative tracking of tumor metabolism and vascular supply, using clinic friendly and portable devices that can monitor deep lesions (multiple centimeters below the skin) in both breast tissue and at the site of bone metastases. During year 2 of the project we have make substantial improvements and advancements in our small imaging technologies, including hyperspectral SFDI and long-wavelength SFDI. The growth rates and feasibility of use of several breast cancer cell-lines/tumor models has been evaluated, with one good option, the Py230 cell lines, as our choice for use in future studies. We have conducted the first study using combined SFDI and multiphoton intravital imaging in a mouse mammary tumor model. Development of a clinical imaging platform has also progressed. Two publications, numerous seminar talks and conference talks and posters have been delivered over the past year to disseminate the work conducted in this award.

15. SUBJECT TERMS

metastases, drug resistance, imaging, optics, diffuse optical imaging, spatial frequency domain imaging, intravital microscopy, therapy monitoring

16. SECURITY CLASSIFICATION OF:			17. LIMITATION OF ABSTRACT	18. NUMBER OF PAGES	19a. NAME OF RESPONSIBLE PERSON
a. REPORT	b. ABSTRACT	c. THIS PAGE			USAMRMC
Unclassified	Unclassified	Unclassified	Unclassified	34	19b. TELEPHONE NUMBER *(include area code)*

Table of Contents

Page

1. **INTRODUCTION:** This project involves the development of optically guided multi-agent therapies for metastatic and drug resistant breast cancer. Non-invasive Diffuse Optical Imaging technologies are able to monitor drug response and resistance through quantitative tracking of tumor metabolism and vascular supply, using clinic friendly and portable devices that can monitor deep lesions (multiple centimeters below the skin) in both breast tissue and at the site of bone metastases. To demonstrate our strategy, we will show, for the first time, that non-invasive optical guidance can enhance the efficacy of combined cytotoxic and antiangiogenic therapy while simultaneously increasing the time until relapse and decreasing toxicities associated with high drug dosing. This will be accomplished without the use of exogenous contrast agents or dedicated imaging facilities. Additionally, in order to demonstrate the feasibility of translating optical signatures discovered in animal models to breast cancer patients, we will conduct a clinical study of non-invasive optical monitoring of drug response.
2. **KEYWORDS:** *drug resistance, imaging, optics, diffuse optical imaging, spatial frequency domain imaging, intravital microscopy, multiphoton imaging, therapy monitoring, metastases,*
3. **ACCOMPLISHMENTS:**

- **What were the major goals of the project?**
  - For reference, the original SOW table is shown below, completed Tasks and Subtasks are shaded in dark blue, ongoing tasks are in lighter blue.

Specific Aim 1: Preclinical Investigation of Systemic Therapies with Optical Imaging	**Timeline**	**Site 1**
Major Task 1: Instrument Setup and Testing	Months	
Subtask 1: Local IACUC Approval	1-3	Dr. Roblyer
Subtask 2: Milestone Achieved: ACURO Approval	3-6	Dr. Roblyer
Milestone #1 ACURO approval obtained	6	Dr. Roblyer
Subtask 3: Custom SFDI Fabrication, order parts and construct device	1-9	Dr. Roblyer
Subtask 4: Setup Multiphoton Microscope, work with vendors to order and install/test microscope	1-9	Dr. Roblyer
Subtask 5: Perform initial SFDI and MPM animal testing with SHO mice and MDA-MB-231 cells. [12 mice x 1 groups = 12 mice]	9-12	Dr. Roblyer
Subtask 6: Evaluate growth rates and treatment response for SHO mice and MDA-MB-231 cells. [12 mice x 1 groups = 12 mice]	6-12	Dr. Roblyer

Milestone #2 SFDI and MPM ready for animal imaging	12	Dr. Roblyer
Major Task 2: Cytotoxic + Antiangiogenic Monitoring		
Subtask 7: Evaluate treatment timelines and response characteristics for SHO mice and MDA-MB-231 cells/ Monitor with SFDI. [18 mice x 3 groups = 54 mice]	12-24	Dr. Roblyer
Subtask 8: Correlate intravital MPM with SFDI [10 mice x 1 groups = 10 mice]	12-24	Dr. Roblyer
Subtask 9: Test growth rates of MMTV-PyMT mice [10 mice x 1 groups = 10 mice]	12-24	Dr. Roblyer
Milestone #3 Define optical signatures of cytotoxic and antiangionic therapy response	24	Dr. Roblyer
Milestone #4 Define quantitative correlates between MPM vascular imaging and SFDI	24	Dr. Roblyer
Major Task 3: Optically Defined Cytotoxic + Antiangiogenic Therapy		
Subtask 10: Test scheduling of cytotoxic + antiangiogenic based on optical signatures. (dependent on Major Task 2) [18 mice x 3 groups = 54 mice]	24-36	Dr. Roblyer
Subtask 11: Additional correlation of intravital MPM and SFDI in optical defined therapeutic window. [10 mice x 1 groups = 10 mice]	24-36	Dr. Roblyer
Subtask 12: Test SFDI and MPM imaging with MMTV-PyMT mice [10 mice x 1 groups = 10 mice]	24-36	Dr. Roblyer
Milestone #5 Improved survival/outcomes though optically defined therapy scheduling	36	Dr. Roblyer
Major Task 4: Early Response Monitoring		
Subtask 13: Test early (hrs) response with SFDI, MPM, IHC, determine immune modulators (dependent on Major Task 2 and 3 results) [18 mice x 3 groups = 54 mice]	36-48	Dr. Roblyer
Milestone #5 Characterize immune modulators of early optical response to systemic therapy.	48	Dr. Roblyer
Major Task 5: New Therapy Monitoring		
Subtask 14: Test optical signatures of response to her2/hormone and/or immunotherapies. (dependent on Major Task 2,3 and 4 results) [18 mice x 3 groups = 54 mice]	48-60	Dr. Roblyer
Milestone #6 Define optical response of new therapies.	60	Dr. Roblyer

Specific Aim 2: In-vivo Clinical Study of Progressive Resistance		
Major Task 6: dDOS fabrication		
Subtask 15: Design/Fabricate dDOS system and new custom dDOS probe	6-24	Dr. Roblyer
Milestone #7 Clinical Ready dDOS system	24	Dr. Roblyer
Major Task 7: Normal Volunteer Study		
Subtask 15: Local IRB Approval (for both normal volunteers and clinical study)	30-33	Dr. Roblyer
Subtask 16: HRPO Approval	33-36	Dr. Roblyer
Subtask 17: Measure 10 normal volunteers with appropriate updates to probe. Analyze and interpret imaging data. [10 normal volunteers]	36-48	Dr. Roblyer
Milestone #8 Normal Volunteer Study Completed and dDOS system/probe ready for clinical study.	48	Dr. Roblyer
Major Task 4:Breast Cancer Clinical Study		
Subtask 18: Measure 30 breast cancer patients. [30 breast cancer patients]	36-57	Dr. Roblyer
Subtask 19: Analyze and interpret imaging data.	36-60	Dr. Roblyer
Milestone #9 Clinical Study Completed, Results Published	60	Dr. Roblyer

- Completion dates for subtasks are listed here:
    - Subtask 1: Local IACUC Approval: 5/31/2016
    - Subtask 2: ACURO Approval: 8/17/2016
    - Subtask 3: Custom SFDI Fabrication: ongoing
    - Subtask 4: Setup Multiphoton Microscope: 8/1/2016
    - Subtask 5: Initial SFDI and MPM testing: 7/1/2017
    - Subtask 6: Evaluate growth rates: 7/1/2017
    - Subtask 7: Treatment monitoring with SFDI: ongoing
    - Subtask 8: Correlate intravital MPM with SFDI: ongoing
    - Subtask 9: Evaluate growth rates: 7/1/2017

- **What was accomplished under these goals?**
    - **Major accomplishments and results are listed for each project goal for year *2* as stated in the subtasks in the SOW. Note: updates from year 1 for completed tasks are not included in this report.**

- **Subtask 3**: In prior reports, updates on custom SFDI Fabrication, including new angle correction algorithms and other technical updates were provided. Here we provide additional updates. It is of note that this subtask has become a fruitful instrumentation development aspect of the project, and will likely continue throughout the award period.
    - A manuscript describing a new way to conduct simultaneous multi-wavelength (hyperspectral) Spatial Frequency Domain Imaging (SFDI) has been published (see appendix).
    - **SFDI short-wave infrared instrument development:** SFDI has been developed to measure wavelengths spanning from the near-infrared to the short-wave infrared (approx. 690nm – 1300nm). This allows for the extraction of quantitative chromophore concentrations of oxy and deoxyhemoglobin, water, and lipids. These parameters are highly relevant to oncology. A manuscript is current in progress describing this new technique. Below is a diagram of the system along with imaging processing steps.

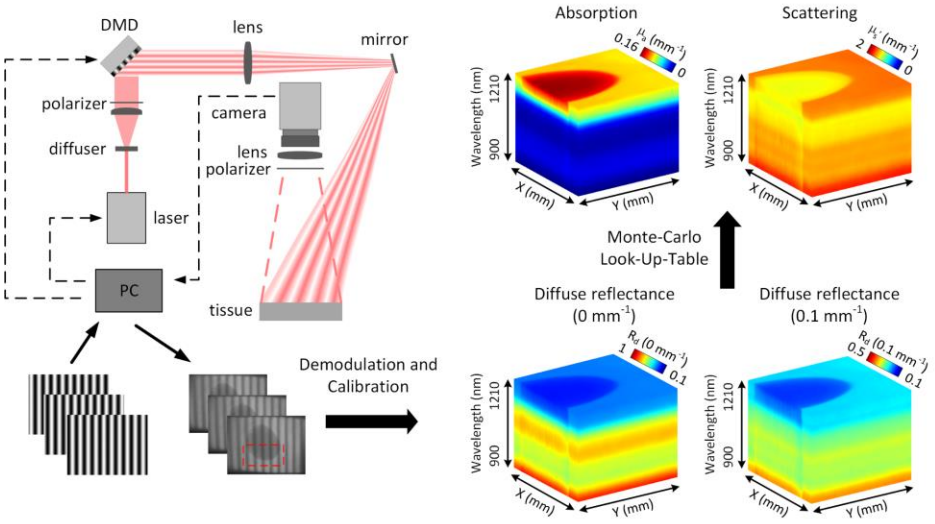

The figure below shows SWIR SFDI data collected from resected mouse tumors, showing that water and lipids can be mapped over the cut tumor surface. This is novel, and will likely lead to new ways to quantify tumor heterogeneity in both the preclinical and clinical settings.

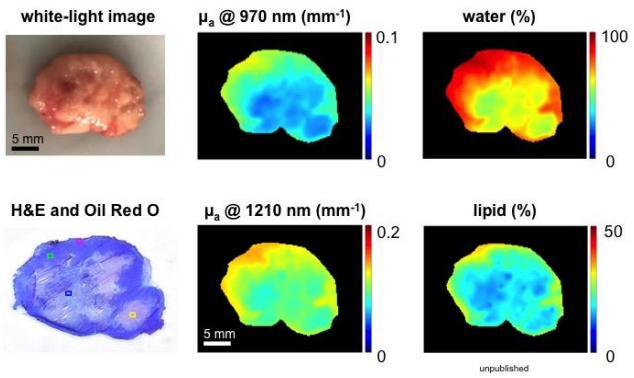

Subtask 6: *Evaluate growth rates and treatment response for SHO mice and MDA-MB-231 cells*.

- Initial *in vitro* IC50 cytotoxicity testing has been conducted for two MMTV-PyMT breast cancer cell lines. As described in detail in section 5, we have now decided to use MMTV-PyMT derived cell lines rather than the MDA-MB-231 cell lines. We have found that the Py230 cell line (triple negative, murine, mesenchymal) grow too rapidly in vivo and form scars and have a very poor take-rate (approximately 50%). We found that the Py8119 cell line (murine, epithelial), are slow-growing, do not form scars, and have almost a 100% take rate. The decision was made to move forward with the use of this cell line for portions of the future work.

Subtask 7: *Evaluate treatment timelines and response characteristics for SHO mice and MDA-MB-231 cells/ Monitor with SFDI.*

- This subtask is ongoing and may involve the use of Herceptin responsive and Herceptin resistance cell lines.

Subtask 8: *Correlate intravital MPM with SFDI*

- Correlations between microvascular architecture (e.g. vascular density, tortuosity, etc.) imaged using intravital MPM and global hemoglobin levels are currently being analyzed in a cohort of mice with Py230 tumors. A figure showing this type of imaging and analysis is shown below. A manuscript is currently in preparation to describe this multiscale imaging procedure.

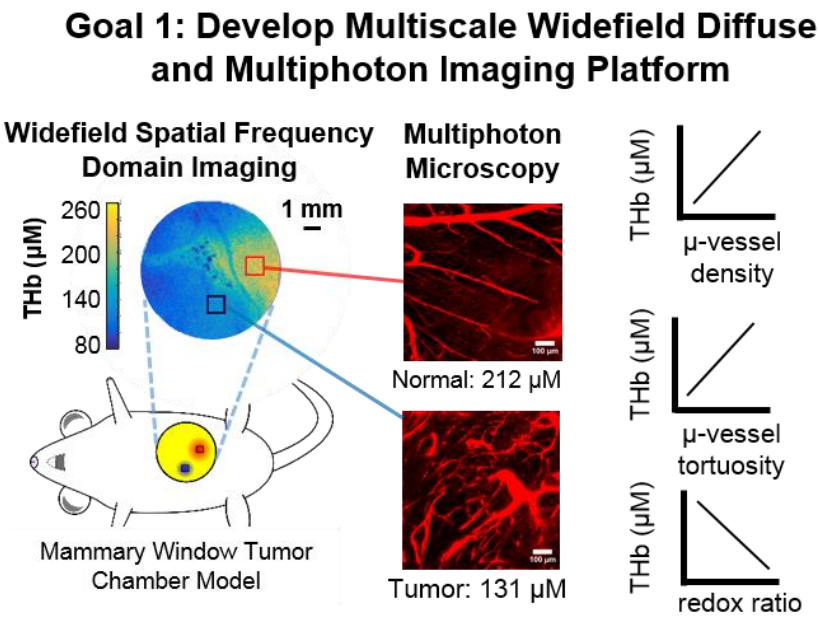

Subtask 9: *Test growth rates of MMTV-PyMT mice*

- The growth rates Py8119 cell line (murine, epithelial) have been characterized.

Subtask 15: *Design/Fabricate dDOS system and new custom dDOS probe*

- Circuits have been designed and printed circuit boards are currently being laid out. New laser sources for the clinical system are being tested. New detector modules are being designed and fabricated.

- **Additional Items not explicitly covered in Subtasks**:
  - Significant training and protocol optimization has been conducted for immunohistochemistry (IHC). These procedures will be important as the project goes forward as many imaging parameters will require validation with IHC and molecular markers tissue testing.

- **What opportunities for training and professional development has the project provided?**
- All Ph.D. students and postdocs attend weekly lab meetings where they present their research results and have regular meeting with the Ph.D. Advisor (Roblyer)
- All Ph.D. students and postdocs attend Journal Club meetings where a different student presents a relevant paper in breast cancer and/or biomedical optics, accompanied by group discussions.

- Several Ph.D. students attended or gave presentations at research conferences over the past year as described in section 6.
- The PI (Roblyer), gave multiple invited seminars listed in section 6.

- **How were the results disseminated to communities of interest?**
    - Results were disseminated through peer-reviewed publications, conference presentations, and invited seminar, listed under part 6: Products.
- **What do you plan to do during the next reporting period to accomplish the goals?**

  The next major push for the project is to utilize the new imaging technology development to start to define optical signatures of chemo-response and chemo-resistance, as well as define how different therapy schedules elicit different biological responses (immunologic versus antiangiogenic). In order to do this, during the next reporting period, we plan to complete subtask 8, culminating in a publication (in preparation), continue work on Subtask 3 with publication (in preparation), continue work or start work on subtasks 7,10,11,12.

4. **IMPACT:** *Describe distinctive contributions, major accomplishments, innovations, successes, or any change in practice or behavior that has come about as a result of the project relative to:*

- **What was the impact on the development of the principal discipline(s) of the project?**
  - The development of SWIR SFDI is likely to have an impact on the field of diffuse optical and preclinical oncology imaging, as deeper tissue penetration as well as the ability to quantify new chromophores, including lipids and collagen, may be highly relevant to chemotherapy and resistance monitoring.
  - The development of hyperspectral multi-wavelength SFDI will likely impact both preclinical and clinical diffuse optical procedures as our recently published procedure is rapid and is not sensitive to ambient lighting conditions.
- **What was the impact on other disciplines?**
  - As the project is still early, there is nothing to report at this time.
- **What was the impact on technology transfer?**
  - Nothing to Report.
- **What was the impact on society beyond science and technology?**
  - The project has the aim of impacting society by improving the health and survival of breast cancer patients.

5. **CHANGES/PROBLEMS:**

- **Changes in approach and reasons for change**
  - This change was previously included in past quarterly reports: Additional literature review and discussions with other researchers have taken place relation to the choice of animal models. In the last progress report we had decided to alter the animal models from the MDA-MB-231 (cell line) SCID Hairless Outbred (SHO) mouse model to a syngeneic mammary mouse model (Balb/c mouse) with either 4T1 or EMT6 mouse mammary tumor cell lines. The cell lines are current being tested for growth rates and chemosensitivity using MTT assay. However, we have learned that both the 4T1 and EMT6 are fast growing and often develop scars on the skin covering the tumor, which is a major barrier for animal imaging. In addition to these two cell lines we have now investigated two additional cell lines derived from the MMTV-PyMT spontaneous breast mouse model to determine if their growth characteristics are more favorable. One of these cell lines, the Py230, has favorable characteristics and is/was used for subtasks 5, 6, 7, 8, and 9. This is a change in the specific cell line, but not in the overall project goals.
  - For subtasks 7,10,11,12 and 13, the goals of these tasks has been further elucidated. For subtasks 7,10,11,12 we will define optical signatures of Herceptin chemo-response and chemo-resistance. For subtask 13 we will define how different therapy schedules elicit very different biological responses (immunologic versus antiangiogenic). These goals are consistent with the original proposal plan.
  - Although not planned until year 3 of the study, based on current accrual trends with our clinical collaborators at the Boston Medical Center for different projects, the number of target subjects for the clinical study may need to modified, or an additional clinical site may need to be added to the study in order to reach the n=30 target accrual. Additional, we are currently considering measuring ex-vivo specimens with hyperspectral SFDI. More investigation into accrual limitations and other clinical sites will be explored over the next year to mitigate changes to the target accrual.
- **Actual or anticipated problems or delays and actions or plans to resolve them**
  - There have been minor delays in several of the subtasks, but we believe this is well balanced by several unanticipated positive results and observations with probable additional publications likely to stem from the work.
- **Changes that had a significant impact on expenditures**
- Nothing to Report.

- **Significant changes in use or care of human subjects, vertebrate animals, biohazards, and/or select agents.** Nothing to Report.
- **Significant changes in use or care of human subjects:** Nothing to Report.
- **Significant changes in use or care of vertebrate animals.** Nothing to Report.
- **Significant changes in use of biohazards and/or select agents.** Nothing to Report.

6. **PRODUCTS:**

- **Publications, conference papers, and presentations**
  - **Journal publications.**

M Applegate, **Darren Roblyer,** *"High-speed Spatial Frequency Domain Imaging (SFDI) with temporally modulated light,"* Journal of Biomedical Optics, 22(7), 076019 (2017) published, *acknowledgement of federal support (yes).*

A Torjesen, R Istfan, **Darren Roblyer**, *"Ultrafast wavelength multiplexed broad bandwidth digital diffuse optical spectroscopy for in vivo extraction of tissue optical properties,"* Journal of Biomedical Optics, 22(3), 036009 (2017) published, *acknowledgement of federal support (yes).*

  - **Books or other non-periodical, one-time publications.**

M Wall, T Heaster, K Tilbury, WJ Choi, **Darren Roblyer**, R Wang, M Skala, J.T.C. Liu, *"Chapter 5: Metabolic Imaging Approaches: Optical Imaging", Imaging and Metabolism,* Jason S. Lewis and Kayvan R. Keshari (Editors), Springer Nature, in production

  - **Other publications, conference papers, and presentations.**

The following invited seminar talks were given by the PI over the last year and data related to this project was featured:

INVITED SEMINARS:

- 07/2017 Wellman Center for Photomedicine, Massachusetts General Hospital, Summer Institute for Biomedical Optics Seminar, Boston, MA
- 06/2017 Johns Hopkins University, Biomedical Engineering Seminar, Baltimore, MD
- 04/2017 Notre Dame, Electrical Engineering Seminar, South Bend, IN
- 03/2017 Rutgers University, Biomedical Engineering Seminar, New Brunswick, NJ
- 02/2017 Norway University of Science and Technology (NTNU), Physics Department Seminar, Trondheim, Norway
- 02/2017 Oslo and Akershus University College (HiOA), Research Seminar, Oslo, Norway
- 01/2017 Columbia University, Research Seminar, SPIE/OSA Student Chapter

INVITED CONFERENCE PRESENTATIONS:

Darren Roblyer, "Personalized and Precision Medicine in Oncology.", ECI Advances in Optics for Biotechnology, Medicine, and Surgery XV, Snowmass, Colorado, July 2017, invited panel presentation and discussant

Darren Roblyer, Raeef Istfan, Alyssa Torjesen, “Wearable high-speed frequency domain diffuse optical imaging for dynamic tumor monitoring.”, OSA Biomedical Optics & Photonics Congress: Optics in the Life Sciences, San Diego, California, April 2017, invited oral presentation

Darren Roblyer, Alyssa Torjesen, Raeef Istfan, Rachita Chaudhury, “Ultra-fast frequency domain Diffuse Optical Spectroscopy using miniaturized sources and detectors towards quantitative wearables”, SPIE Photonics West, San Francisco, California, February 2017, invited oral presentation

Darren Roblyer, Syeda Tabassum, Junjie Wu, David J. Waxman, “Spatial frequency domain imaging (SFDI) as a new tool for monitoring chemotherapy response and resistance”, SPIE Photonics West, San Francisco, California, February 2017, invited oral presentation

CONFERENCE PRESENTATIONS:

Presenter listed as first author
M Applegate, Darren Roblyer, “High-speed Spatial Frequency Domain Imaging (SFDI) with temporally modulated light.”, ECI Advances in Optics for Biotechnology, Medicine, and Surgery XV, Snowmass, Colorado, July 2017, poster presentation

V Pera, K Karrobi, S Tabassum, Darren Roblyer, “Exploiting diffuse reflectance measurement uncertainty estimates in spatial frequency domain imaging.”, ECI Advances in Optics for Biotechnology, Medicine, and Surgery XV, Snowmass, Colorado, July 2017, poster presentation

HM Peterson, BH Hoang, D Geller, R Gorlick, R Yang, J Berger, J Tingling, M Roth, J Gill, Darren Roblyer, “Clinical Feasibility of Chemotherapy Monitoring for Bone Sarcoma Patients with Diffuse Optical Spectroscopic Imaging ”, American Association for Cancer Research (AACR) Annual Meeting, Washington D.C., April 2017, poster presentation

Yanyu Zhao, Kavon Karrobi, John P. Dumas, Mark C. Pierce, Darren Roblyer, “Hyperspectral spatial frequency domain imaging from 680-1,300 nm for improved estimation of tissue water and lipid concentrations”, SPIE Photonics West, San Francisco, California, February 2017, oral presentation

- **Website(s) or other Internet site(s)**

  Lab website: www.bu.edu/botlab

- **Technologies or techniques**

  Identify technologies or techniques that resulted from the research activities. In addition to a description of the technologies or techniques, describe how they will be shared.

  - A new way to conduct simultaneous multi-wavelength (hyperspectral) Spatial Frequency Domain Imaging (SFDI) has been developed and published. This system is described in detail in section 3, under the research update for subtask 3.
  - A new SFDI near infrared (NIR) and short wave infrared (SWIR) system was developed. This system is described in detail in section 3, under the research update for subtask 3.

- **Inventions, patent applications, and/or licenses**

  Nothing to Report.

- **Other Products**

  - *All relevant results and products have been described in previous sections.*

7. PARTICIPANTS & OTHER COLLABORATING ORGANIZATIONS

- **What individuals have worked on the project?**

Name:	*Darren Roblyer*
Project Role:	*PI*
Researcher Identifier (era Commons ID):	*droblyer*
Nearest person month worked:	*2*
Contribution to Project:	*Overall project management, data analysis, mentorship*
Funding Support:	DOD

Name:	*Irving Bigio*
Project Role:	*Collaborator*
Researcher Identifier (era Commons ID):	*ijbigio*
Nearest person month worked:	*1*
Contribution to Project:	*Mentor and collaborator. Provides technical support and feedback for optical instrumentation.*
Funding Support:	DOD

Name:	*David Waxman*
Project Role:	*Collaborator*
Researcher Identifier (era Commons ID):	*David_Waxman*
Nearest person month worked:	*1*
Contribution to Project:	*Mentor and collaborator for small animal studies and IHC.*
Funding Support:	DOD

Name:	*Fei Teng*
Project Role:	*Graduate Student*
Researcher Identifier (era Commons ID):	*na*
Nearest person month worked:	*4*
Contribution to Project:	*Working on clinical diffuse optical technologies*
Funding Support:	*DOD*

Name:	*Kavon Karrobi*
Project Role:	*Graduate Student*
Researcher Identifier (e.g. ORCID ID):	na
Nearest person month worked:	12
Contribution to Project:	*Working on multiphoton intravital imaging as well as custom SFDI instrumentation.*
Funding Support:	DOD

Name:	*Wei-Han Liu*
Project Role:	*Graduate Student*
Researcher Identifier (e.g. ORCID ID):	na
Nearest person month worked:	*4*
Contribution to Project:	Worked on scattering signatures of chemotherapy response
Funding Support:	DOD

Name:	*Yanyu Zhao*
Project Role:	*Graduate Student*
Researcher Identifier (e.g. ORCID ID):	na
Nearest person month worked:	11
Contribution to Project:	Worked on SWIR SFDI instrumentation and testing
Funding Support:	DOD

Name:	*Alyssa Torjesen*
Project Role:	Worked on clinical diffuse optical instrumentation
Researcher Identifier (e.g. ORCID ID):	na
Nearest person month worked:	*2*
Contribution to Project:	
Funding Support:	DOD

Name:	*Vivian Pera*
Project Role:	*Postdoctoral Fellow*
Researcher Identifier (e.g. ORCID ID):	na
Nearest person month worked:	*12*
Contribution to Project:	*Light propagation modeling in biological tissue.*
Funding Support:	DOD

Name:	*Matthew Applegate*
Project Role:	*Postdoctoral Fellow*
Researcher Identifier (e.g. ORCID ID):	na
Nearest person month worked:	*11*
Contribution to Project:	Time-multiplexed SFDI for rapid animal imaging
Funding Support:	DOD

Name:	*Asha Pant*
Project Role:	*Animal Technician*
Researcher Identifier (e.g. ORCID ID):	na
Nearest person month worked:	*5*
Contribution to Project:	*Small animal technician, animal care, cell studies, chemotherapy injections.*
Funding Support:	DOD

- **Has there been a change in the active other support of the PD/PI(s) or senior/key personnel since the last reporting period?**
  - Nothing to Report.
- **What other organizations were involved as partners?**
  - **Organization Name:** Modulated Imaging Inc.
  - **Location of Organization:** *Irvine, CA*
  - **Partner's contribution to the projec**t
    - **Collaboration** *Amman Mazhar and David Cuccia at Modulated Imaging Inc. provide technical support and feedback on imaging techniques throughout the project.*

8. **SPECIAL REPORTING REQUIREMENTS**
    - Not applicable
9. **APPENDICES:**

Journal of Biomedical Optics

BiomedicalOptics.SPIEDigitalLibrary.org

Ultrafast wavelength multiplexed broad bandwidth digital diffuse optical spectroscopy for *in vivo* extraction of tissue optical properties

Alyssa Torjesen
Raeef Istfan
Darren Roblyer

SPIE.

Alyssa Torjesen, Raeef Istfan, Darren Roblyer, "Ultrafast wavelength multiplexed broad bandwidth digital diffuse optical spectroscopy for *in vivo* extraction of tissue optical properties," *J. Biomed. Opt.* **22**(3), 036009 (2017), doi: 10.1117/1.JBO.22.3.036009.

Ultrafast wavelength multiplexed broad bandwidth digital diffuse optical spectroscopy for *in vivo* extraction of tissue optical properties

Alyssa Torjesen, Raeef Istfan, and Darren Roblyer*
Boston University, Department of Biomedical Engineering, Boston, Massachusetts, United States

Abstract. Frequency-domain diffuse optical spectroscopy (FD-DOS) utilizes intensity-modulated light to characterize optical scattering and absorption in thick tissue. Previous FD-DOS systems have been limited by large device footprints, complex electronics, high costs, and limited acquisition speeds, all of which complicate access to patients in the clinical setting. We have developed a new digital DOS (dDOS) system, which is relatively compact and inexpensive, allowing for simplified clinical use, while providing unprecedented measurement speeds. The dDOS system utilizes hardware-integrated custom board-level direct digital synthesizers and an analog-to-digital converter to generate frequency sweeps and directly measure signals utilizing undersampling at six wavelengths modulated at discrete frequencies from 50 to 400 MHz. Wavelength multiplexing is utilized to achieve broadband frequency sweep measurements acquired at over 97 Hz. When compared to a gold-standard DOS system, the accuracy of optical properties recovered with the dDOS system was within 5.3% and 5.5% for absorption and reduced scattering coefficient extractions, respectively. When tested *in vivo*, the dDOS system was able to detect physiological changes throughout the cardiac cycle. The new FD-dDOS system is fast, inexpensive, and compact without compromising measurement quality. [DOI: 10.1117/1.JBO.22.3.036009]

Keywords: diffuse optics; frequency domain; instrumentation; undersampling.

Paper 160873R received Dec. 22, 2016; accepted for publication Feb. 17, 2017; published online Mar. 10, 2017.

1 Introduction

Diffuse optical spectroscopy (DOS) has emerged over the past three decades as an important noninvasive method to characterize optical scattering and absorption and, in turn, calculate chromophore concentrations in thick tissue.[1,2] Diffuse optical methodologies can be broadly categorized into three distinct measurement types: time domain, frequency domain (FD), and continuous wave (CW). This work focuses on FD-DOS, which allows for the separation of optical scattering and absorption through the measurement of amplitude attenuation and phase delay of photon density waves generated by temporally intensity modulated light sources at the tissue surface. Prior FD-DOS systems have utilized either a single modulation frequency[3–9] or a sweep of multiple frequencies[5–7] in the radio frequency (RF) range. Most single modulation frequency systems utilize either homodyne[4,7,8,10] or heterodyne[3] techniques to downconvert the high frequency signal of interest by mixing it with a reference signal. Broad bandwidth DOS instruments, which utilize light sources that are swept through a range of RF frequencies, have typically utilized a benchtop network analyzer to generate and measure signals up to the gigahertz range.[1,11] FD-DOS devices based around network analyzers have relatively large instrument footprints, and the cost of fabrication can range from approximately $30,000 to $60,000 (based on our internal cost estimates), limiting access to patients in the clinic. Although some analog systems have been successfully miniaturized,[12,13] the difficulties involved in RF system design potentially limit the adoption of these techniques. Furthermore, FD-DOS instruments often have slow measurement acquisition speeds compared to their CW counterparts, and although recent improvements have been made in data acquisition rates for single modulation frequency measurements,[14] data acquisition speeds are limited for broad modulation frequency bandwidth FD-DOS systems.[1,10,15]

We recently demonstrated the feasibility of FD-DOS measurements using all digital signal generation and detection using direct digital synthesizer (DDS) integrated circuits and a 3.6-gigasample/s two-channel analog-to-digital converter (ADC).[16] These digital components reduced system costs, but measurement acquisition speed was limited due to data transfer bottlenecks between system components. Furthermore, the high sampling rate of the ADC resulted in large datasets and lengthy data transfer times. A second implementation of a digital FD-DOS system tested the feasibility of utilizing a slower ADC, sampling at only 25 megasamples/s, and utilizing undersampling techniques.[17] This substantially reduced system complexity but measurement speed was still a major limitation due to limited data transfer rates. Here, we present a new FD-DOS system that overcomes these past limitations by fully integrating digital signal synthesis and detection to rapidly acquire multiwavelength, multiplexed, broadband frequency sweep measurements at a repetition rate of up to 97 Hz. The digital DOS (dDOS) system was validated relative to a gold-standard network analyzer based DOS system and tested *in vivo*. This new high-speed, broad-bandwidth, digital, miniaturized DOS system minimizes analog circuitry while reducing cost and device footprint, potentially enabling access to more patients

*Address all correspondence to: Darren Roblyer, E-mail: roblyer@bu.edu

in the clinic and expanding the capabilities of this technology, especially for monitoring fast physiological changes.

2 System Design and Processing

2.1 *Hardware Integration*

Figure 1 shows the core components and signal/data flow for the new dDOS system. The hardware components of the dDOS system are integrated into a single motherboard that both generates and measures RF signals while communicating and transferring data to the host computer. A development board (ZedBoard, MircoZed Zynq-7010 SoC) was used as the central processing and data storage core for the system. It contains an ARM Cortext-A9 processor and an Artix 7 FPGA, 1 GB of RAM to store data read from the ADC, and a Linux server to transfer data between the board and host computer. The user sets the desired frequency sweep settings in software and the Linux server configures the DDS boards accordingly. The two-channel ADC samples both channels simultaneously and transfers data to the RAM on the MicroZed module via a parallel low voltage differential signal bus. Data are then transferred from the Linux server to the host computer via an Ethernet link at a rate of up to 170 Mbps.

2.2 *Light Sources and Modulation*

The dDOS system utilizes NIR laser diodes with wavelengths of 658, 690, 785, 808, 830, and 850 nm that are housed in thermoelectric cooling modules (Thorlabs, LDM9T). All laser diodes are coupled to 400-μm core diameter fibers bundled into a single ferrule. Each laser diode is driven with a DC current, which is mixed with an RF current using a bias-tee to intensity-modulated light. DC current is supplied by an eight-channel, high-stability laser diode controller (ILX Lightwave, LDC-390, Newport Corporation). The dDOS system replaces the RF current output functionality of the network analyzer by implementing six DDS chips (AD9910, Analog Devices), each on individual daughterboards. Each DDS can output up to 20 mA of current modulated up to 400 MHz. The RF output of each DDS board is low-pass filtered at 400 MHz and routed to a 7:1 directional coupler. The directional coupler sends the majority of the output power to the bias-tee, and the lesser output from each directional coupler is routed to a power combiner (Mini-Circuits, ZBSC-615+) and measured as a reference signal with the second channel of the ADC.

The dDOS system is capable of utilizing the six individual DDS chips to simultaneously modulate a bank of laser diodes at offset frequencies. The data are then demultiplexed in the FD in postprocessing. A typical dDOS measurement, for example, may sweep through frequencies between 50 and 400 MHz in steps of 1 MHz with the modulation frequency for each wavelength offset by 10 MHz. This multiplexing reduces measurement duration to less than 100 ms/frequency sweep (in the slowest case), allowing for detection of rapid physiological changes. For this work, modulation frequencies between 50 and 300 MHz or between 50 and 400 MHz were used depending on the optical attenuation of the sample and data acquisition rate requirements. The frequency step size can be set between 1 and 7 MHz. For wavelengths with modulation sweeps starting above 50 MHz, the modulation frequency was incremented up to the maximum frequency then wrapped back to 50 MHz and incremented to the starting frequency. Data were unwrapped such that modulation frequencies appear in increasing order.

2.3 *Detection*

Reflectance mode geometry was used for all dDOS measurements, with the source fiber bundle and active area of an avalanche photodiode (APD) placed directly on the surface of the phantom at a source detector separation of 10 to 30 mm depending on the specific measurement. An APD module (Hamamatsu C5658) with a 0.5-mm active area, 2.50×105 V/W photoelectric sensitivity, and a high band cutoff of 1 GHz was used for most phantom measurements. For *in vivo* experiments, data were acquired with a 3-mm active area APD.

A 14-bit, two-channel ADC (Texas Instruments, ADS62P49) with a 2 V peak-to-peak full-scale input voltage was used to

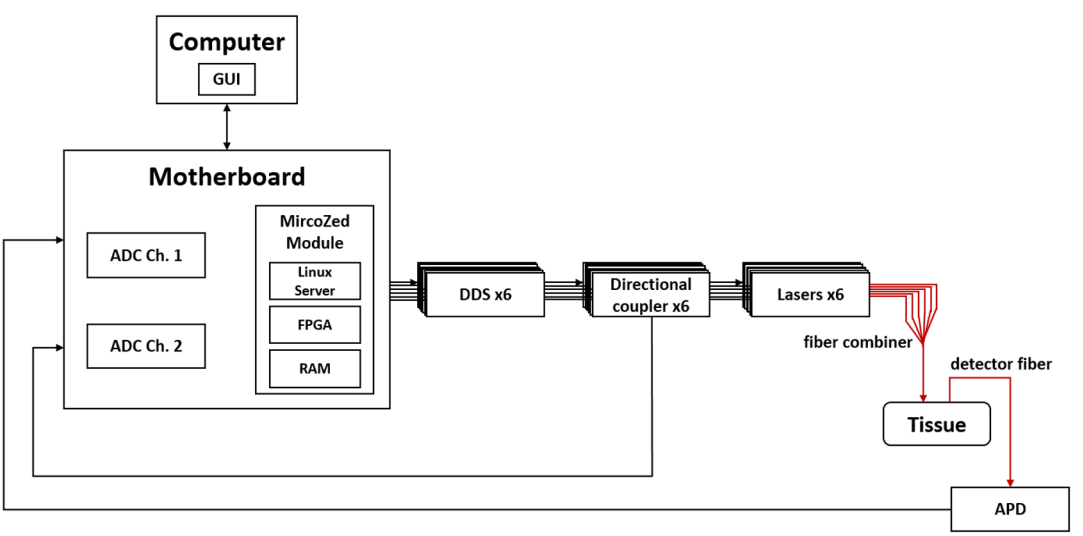

Fig. 1 Schematic overview of dDOS system. GUI, graphical user interface; ADC, analog-to-digital converter; FPGA, field programmable gate array; RAM, rapid access memory; DDS, direct digital synthesizer; APD, avalanche photodiode.

sample the signal at each channel at 250 MSPS. The electrical output of the APD was high-pass filtered at 41 MHz and routed to the first channel of the ADC, while the combined reference signal from the power combiner was routed to the second channel of the ADC. The user can select the number of samples collected by each channel of the ADC at each frequency step (e.g., $4096, 8192, 16384 \ldots 2^n$). Increasing the number of samples per step substantially increases data transfer and processing time. Both channels of the ADC run off of the same clock and are sampled simultaneously.

2.4 *Signal Processing*

All signal processing is performed in MATLAB (R2014b, Mathworks Natick, Massachusetts). Since the two-channel ADC has a sampling rate of 250 MSPS, all signals modulated above 125 MHz are aliased. Given that the modulation frequency is known for each wavelength at each frequency step, the signal of interest is easily located in the baseband. The processing algorithm eliminates modulation frequencies that are multiples of the Nyquist frequency and removes any measurements in which multiple wavelengths are aliased to the same frequency in the baseband (e.g., signals at 120 and 130 MHz are both read as 120 MHz and eliminated).

A fast Fourier transform (FFT) with a rectangular window was used at each frequency step to calculate the amplitude and phase for the reference and sample channels. The appropriate frequency bin was located for each wavelength at each modulation frequency step. The magnitude of the FFT of the measurement channel relative to that of the reference channel was considered the raw amplitude value, and, similarly, the phase offset between the measurement and reference channels was considered the raw phase value.

2.5 *Measurement Calibration and Optical Property Extraction*

The raw amplitude and phase represent the amplitude attenuation and phase delay induced both by the tissue and the instrument. In order to remove the instrument response, a measurement was taken on a silicone phantom with known optical properties, where calibration optical properties were obtained using multidistance measurements. An analytical solution to the P1 approximation of the Boltzman transport equation with boundary conditions for semi-infinite geometry was employed as a forward model for the phantom measurement.[5] Calibration factors for amplitude and phase were determined by ratiometrically or differentially comparing the measured amplitude and phase, respectively, to the theoretical amplitude and phase from the forward model. These calibration factors were then applied to the subsequent raw amplitude and phase measurements in order to obtain calibrated amplitude and phase.

An iterative least-squares fitting algorithm was employed to minimize the error between the forward model calculated and measured calibrated amplitude and phase to extract absorption (μ_a) and scattering (μ_s') parameters at each wavelength.[5] Chromophore extinction coefficients were obtained from Zijlstra and Buursma.[18] The Beer–Lambert law was used to extract chromophore concentrations (oxy- and deoxyhemoglobin) from multiwavelength μ_a data.[13]

3 System Characterization

3.1 *System Overview*

The completed dDOS system is shown in Fig. 2, where the motherboard, DDS daughterboards, MicroZed module, ADC, and RF output connections are pictured. The primary hardware is housed in an enclosure measuring $10 \times 12 \times 6$ in.

3.2 *Signal to Noise*

Signal to noise was measured on a breast-simulating silicone optical phantom. SNR was compared for measurements taken using either a single laser or all six lasers modulated simultaneously. A comparison was also done for measurements taken using either 4096 or 8192 samples. The noise floor was calculated as the average noise level, in dBc, relative to the frequency of interest. Figure 3 shows that when all six lasers were modulated simultaneously, the noise floor was −46.3 dBc, whereas utilizing a single laser yielded a lower noise floor of −50.1 dBc. When increasing the sample length to 8192 samples per frequency step, the noise floor was reduced to −49.2 and −54.5 dBc for multiplexed and single wavelength measurements, respectively. Although the noise floor was lower with 8192 samples per frequency step, acquisition and data transfer times of these measurements were substantially slower than of those with 4096 samples per frequency step, and there was no improvement in accuracy of optical properties (e.g., the accuracy of 10 measurements on two phantoms with 4096 samples per frequency step was 1.29% compared to 1.85% with 8192 samples per frequency step). 4096 samples per frequency step were collected for all subsequent measurements to optimize speed.

3.3 *Accuracy of Optical Property Extractions*

An example of calibrated (black) and fit (red) amplitude and phase measured from 50 to 400 MHz in steps of 1 MHz at each wavelength is shown in Fig. 4. Data were calibrated using a silicone phantom with known optical properties in order to remove the instrument response. Measurements at 658 and 850 nm have somewhat higher noise levels compared to other wavelengths, likely due to the lower modulation index achieved for these laser diodes.

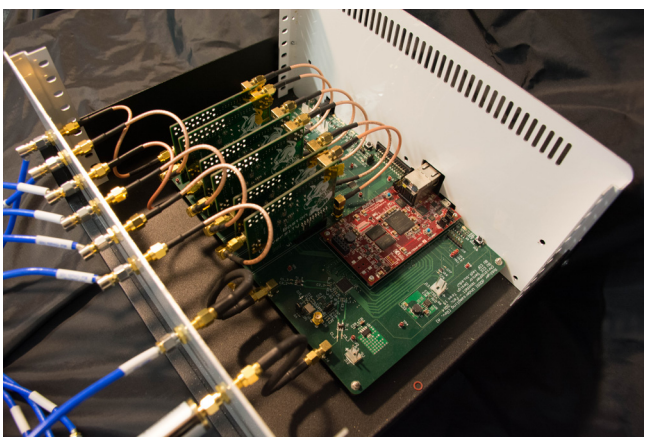

Fig. 2 dDOS core electronics.

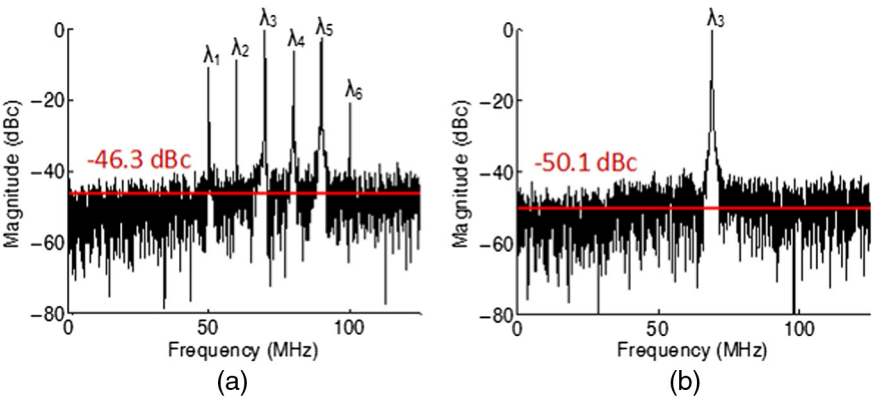

Fig. 3 Noise floor when collecting 4096 samples per frequency step in (b) a single wavelength measurement or (a) a multiplexed measurement with a 10 MHz offset between wavelengths.

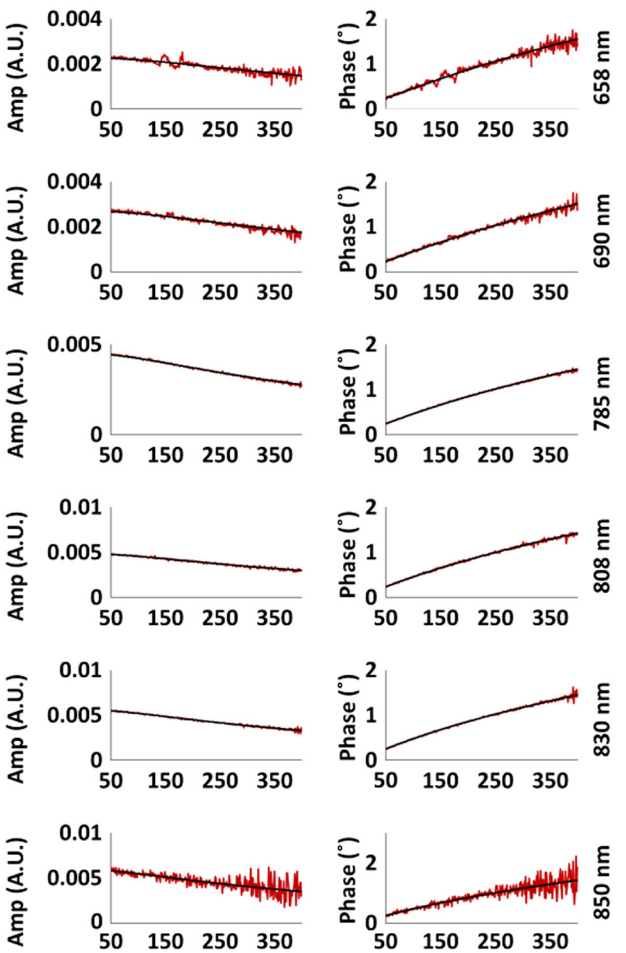

Fig. 4 Amplitude (in arbitrary units, A.U.) and phase measured with dDOS system at each wavelength. Red lines are calibrated data and black lines are model fits.

dDOS optical property extraction accuracy was determined by measuring a set of 10 tissue-simulating silicone phantoms with varying amounts of titanium dioxide and nigrosin, as the scattering and absorbing agents, respectively, using both the dDOS and the network analyzer-based benchtop DOS systems. For each phantom, 10 FD measurements were taken with each system with a 15-mm source–detector separation and all six wavelengths modulated at frequencies between 50 and 400 MHz with 1-MHz frequency steps. Measurements on one highly attenuating phantom at 658, 690, and 850 nm were excluded due to phase errors resulting from low detected signal levels. The mean of the absolute difference in optical properties for all measured phantoms between the two systems was 5.3% and 5.5% for μ_a and μ_s', respectively; when frequency sweeps from 50 to 300 MHz were used, the mean accuracy in optical properties measured with the two systems was 4.9% and 6.0% for μ_a and μ_s', respectively.

Figure 5 shows scatterplots (top panels) and Bland–Altman plots (bottom panels) for μ_a and μ_s' measured with the dDOS and benchtop DOS systems. For the Bland–Altman plots, the differences between optical properties with the dDOS and benchtop system are plotted on the y-axis versus average optical properties for each system on the x-axis, for each wavelength and phantom. 96% of μ_a measurements and 98% of μ_s' measurements fell within 1.96 standard deviations of the mean difference, indicating acceptable equivalence between the two systems.[19] μ_a and μ_s' both tend to skew slightly lower for the dDOS system compared to the benchtop DOS system. μ_a values had the best agreement between systems when the mean absorption coefficient was <0.015 mm^{-1}, while μ_s' had the best agreement between systems when the mean reduced scattering coefficient was >1 mm^{-1}. In healthy breast tissue, μ_a in the NIR is typically <0.01 mm^{-1} and μ_s' in the NIR is typically >0.8 mm^{-1}.[20]

3.4 *Precision*

The stability of amplitude, phase, and optical properties was characterized during a 2-h drift test. Measurements were taken at ~1-min intervals on a silicone optical phantom using 658, 690, 785, 808, 830, and 850 nm lasers modulated simultaneously in frequency sweeps from 50 to 400 MHz with a 15-mm source–detector separation. Amplitude and phase were examined for the duration of the drift test for the 850-nm laser modulated at 50 MHz and were plotted in Fig. 6. For this wavelength and modulation frequency, the standard deviation of the phase was 0.38 deg and the standard deviation of the amplitude relative to the mean amplitude was 0.81%.

System stability was further analyzed for all wavelengths and modulation frequencies used in the drift test, and results are shown in Table 1. Amplitude and optical property stability were defined as the standard deviation divided by the mean

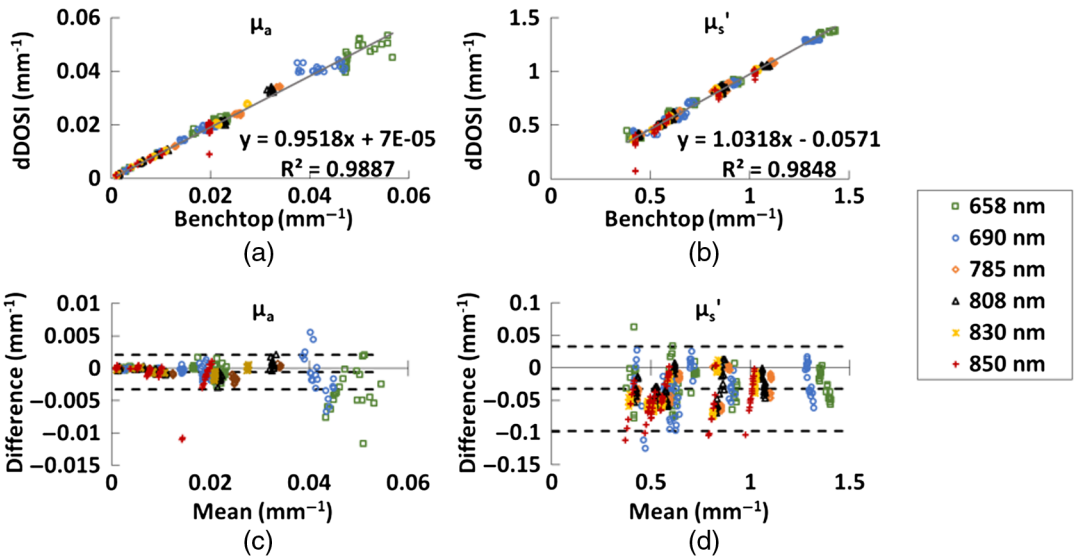

Fig. 5 (a and b) Scatterplots and (c and d) Bland–Altman plots of optical properties obtained with the dDOS system compared to those obtained with the benchtop system. Top and bottom dashed lines represent 1.96 standard deviations from the mean difference; center dashed lines represent the mean difference.

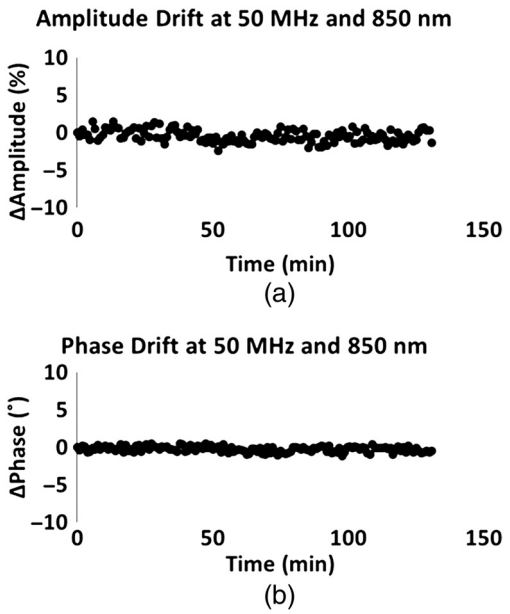

Fig. 6 2-h drift test showing dDOS system stability. Measurements were taken approximately every minute and show variation from value at the first time point ($t = 0$). (a) Amplitude drift at 50 MHz and 850 nm and (b) phase drift at 50 MHz and 850 nm.

Table 1 System stability during a 2-h drift test with measurements taken approximately every minute.

Average stability across all wavelengths and modulation frequencies	
Amplitude	1.0%
Phase	1.7 deg
μ_a	2.0%
μ_s'	0.8%

at each modulation frequency, averaged for all wavelengths. Phase stability was defined as the standard deviation throughout the drift test averaged for all wavelengths and modulation frequencies. The stability in μ_a and μ_s' was 2.0% and 0.8%, respectively.

3.5 *Speed*

Most prior FD-DOS instruments performed frequency sweeps with each wavelength modulated individually in a sequential manner.[5,17] The dDOS system utilizes wavelength multiplexing, which eliminates switching time between lasers and reduces data acquisition time, resulting in the ability to measure fast physiological changes. The rate at which frequency sweep measurements can be performed is dependent on the range of modulation frequencies, the step size, and the number of samples acquired at each frequency step. When multiplexing six laser wavelengths, sweeping from 50 to 300 MHz with 7 MHz steps, and acquiring 4096 samples per frequency step, the maximum speed achieved for dDOS system was 97.2 Hz. Increasing the frequency sweep range from 50 to 400 MHz reduces the measurement rate to 68.1 Hz. When decreasing the frequency step size to 1 MHz, the 50 to 300 MHz sweep can be acquired at 13.9 Hz, and the 50 to 400 MHz sweep can be acquired at 9.8 Hz. These measurement speeds allow for FD-dDOS data acquisition that can capture fast physiological changes, including during the cardiac cycle.

To test the maximum measurement speed attainable with the dDOS system, measurements were also taken with a single modulation frequency. When modulating at only 50 MHz, a measurement rate of 2557 Hz can be achieved. Although this is not the preferred data acquisition mode, because utilizing additional modulation frequencies improves model fit accuracy, it provides a useful comparison to other FD systems, which utilize single modulation frequencies.[3,4,8,10,14,21]

A summary of the performance specifications is given in Table 2.

Table 2 dDOS performance specifications.

dDOSI performance summary	
SNR (typical)	46.3 dBc
μ_a accuracy	5.3%
μ_s' accuracy	5.5%
Phase stability	1.7 deg
Amplitude stability	1.0%
Measurement rate (50 to 300 MHz sweeps)	97.2 Hz
Maximum measurement rate (single frequency)	2557 Hz

4 In Vivo Testing

All *in vivo* human measurements were carried out under a protocol approved by the Boston University Institutional Review Board.

4.1 *Cuff Occlusion Measurement*

An *in vivo* cuff occlusion measurement was performed using a blood pressure cuff placed on the upper arm of a male volunteer, while optical measurements were taken on the forearm. The cuff was loosely secured in order to measure baseline molar concentrations of oxyhemoglobin (ctO_2Hb) and deoxyhemoglobin (ctHHb). The cuff was then was inflated to 200 mmHg for ~2 min, and then released and data were acquired for ~5 additional minutes. Frequency sweeps between 50 and 400 MHz, with frequency steps of 1 MHz, were used to modulate all six laser diodes simultaneously. Measurements were taken approximately every 8 s for 10 min and a source–detector separation of 10 mm was used for each measurement.

Figure 7 shows ctO_2Hb and ctHHb throughout the cuff occlusion test. At baseline average, ctO_2Hb and ctHHb were 41.6 and 41.2 μM, respectively. At the time of cuff release, ctO_2Hb had dropped to 19.3 μM and ctHHb had increased to 87.6 μM. After cuff release, ctO_2Hb rebounded to a local maximum of 67.7 μM and ctHHb dropped to 36.5 μM, before both chromophore concentrations began to return toward their baseline values. These results are consistent with reduced arterial supply and vascular drainage during cuff occlusion, followed by a rush of arterial blood into the forearm after cuff release.

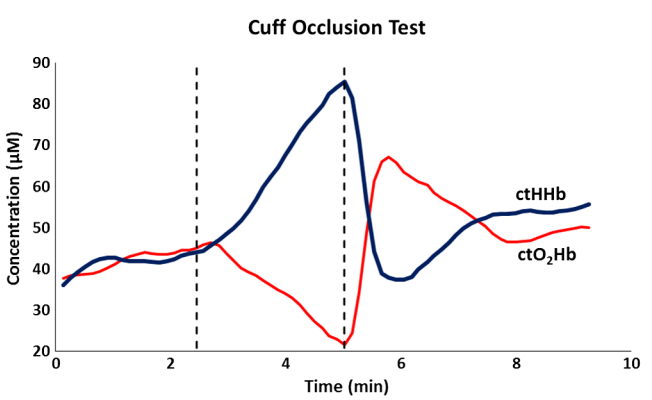

Fig. 7 Forearm cuff occlusion test. Cuff was occluded during time interval between dashed lines. Measurements were taken approximately every 8 s and a three-point moving average is plotted for each chromophore.

4.2 *Rapid In Vivo Measurements*

To test the ability of the dDOS system to measure physiological changes at the cardiac rate, frequency sweep measurements were taken on the finger of a male volunteer. Measurements were taken in reflectance mode on the index finger with a 10-mm source–detector separation. Frequency sweeps from 50 to 300 MHz with 7 MHz steps were used to modulate all six laser diodes simultaneously. About 350 frequency sweeps were taken with a measurement rate of 97.2 Hz.

An electrocardiogram (ECG) signal was measured simultaneously with the optical signal and synced using an external data acquisition board. Figure 8 shows five-point moving averages of μ_a, μ_s', ctTHb, ctO_2Hb, and ctHHb from the high-speed finger measurement temporally aligned with the ECG. μ_a values fluctuate temporally with the ECG signal, likely due to increased blood volume in the finger after ventricular contraction. Similarly, ctTHb and ctO_2Hb vary temporally with the ECG signal, while ctHHb shows minimal fluctuation throughout the cardiac cycle. Vertical dashed lines mark the peak of the ECG R-wave, the start of the upstroke of the pulsatile waveform, and the dicrotic notch. There is a 155-ms lag in the upstroke of the μ_a signal after the R-wave of the ECG, due to the transmission time of the pressure wave to the peripheral vasculature. The delay is often referred to as the pulse transit time and previously shown to range between 200 and 300 ms for photoplethysmographic signals measured in the fingertip.[22] The dicrotic notch, which is correlated with end of the systolic ejection period, is likely correlated with the dip in μ_a, ctTHb and ctO_2Hb marked by the rightmost vertical line. In this case, the dichrotic notch appears roughly 303 ms after the upstroke of the pulsatile waveform, in agreement with other report values in the literature.[23,24] Fluctuations in μ_a, ctTHb, and ctO_2Hb appear to occur at the same frequency as the ECG signal, suggesting that the dDOS system is capable of detecting pulsatile, oxygenated, arterial blood flow.

4.3 *Chromophore Maps in Healthy Breast Tissue*

Optical properties of breast tissue were measured on a healthy female volunteer. Measurements were taken with the dDOS system using 658, 690, 785, 808, 830, and 850 nm lasers with a 28-mm source–detector separation and modulation frequencies from 50 to 400 MHz. 36 point measurements were taken in which the source–detector pair was manually scanned across the right breast in a 6×6 cm grid pattern with 1 cm spacing between measurement points. A quadrant of the areolar complex was located at the top left corner of the imaging grid. Optical properties were calculated and chromophore values determined for each data point. Data from the 658- and 850-nm wavelengths were excluded due to noise in the phase measurement at these wavelengths. Figure 9 shows a chromophore map for ctTHb with linear interpolation between measurement points. The chromophore map was superimposed on a 3-D scanned bust model in order to show the approximate relative position of the measurement. There is a region of increased ctTHb at the top left corner of the chromophore map, likely due to increased

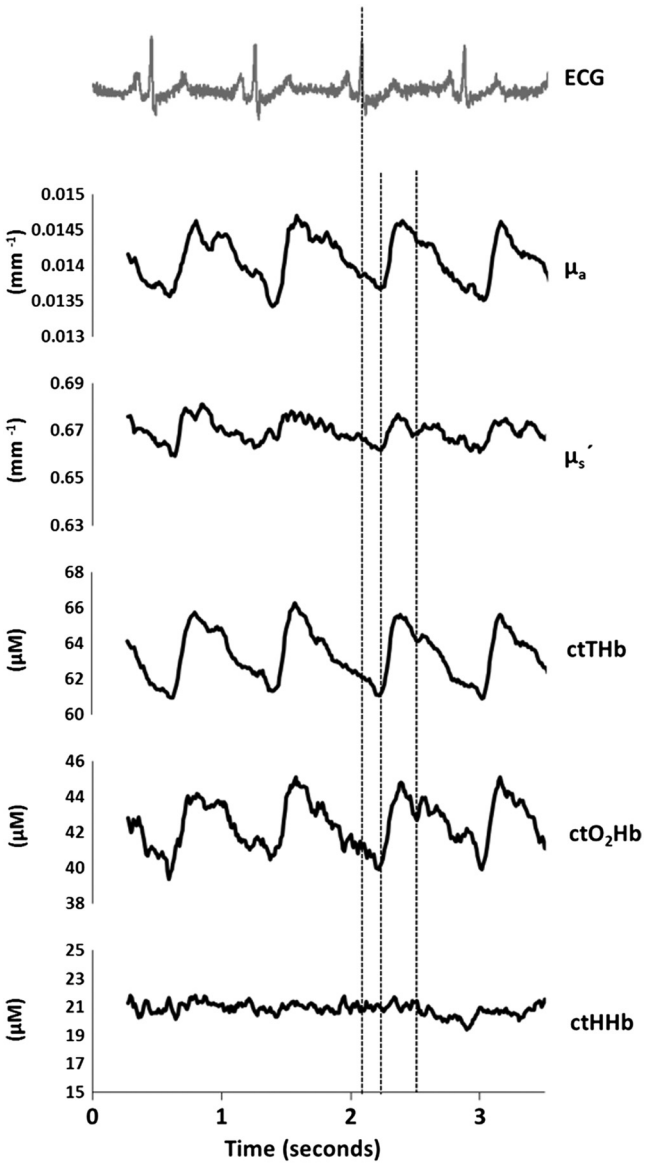

Fig. 8 High-speed dDOS measurements were taken on the index finger. An ECG signal was obtained simultaneously with the optical measurements and temporally aligned with optical property and chromophore values. From top to bottom, plots represent the ECG, μ_a, μ_s', ctTHb, ctO_2Hb, and ctHHb. The leftmost vertical dashed line represents the approximate time of the peak of the ECG R-wave, the middle dashed line represents the approximate time of the start of the upstroke of the optical signal following the arterial transit time, and the rightmost dashed line represents the approximate timing of the dicrotic notch based on visual inspection.

blood supply to the areola as compared to standard breast tissue, which has been observed in prior DOS studies.[25]

5 Discussion

A new dDOS system was developed to increase access to patients, while adding new capabilities in measurement speed. Traditional network analyzer-based FD-DOS systems are large and costly, and miniaturization of analog RF circuits is technically challenging. The hardware-integrated dDOS system developed here utilizes direct digital signal generation and detection and wavelength multiplexing, with frequency sweep measurements rates up to 97 Hz, allowing rapid physiological changes

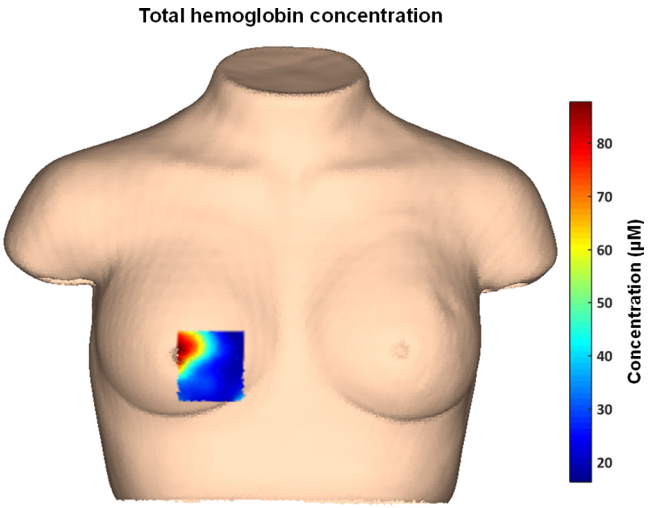

Fig. 9 ctTHb measured on the right breast of a healthy volunteer. A quadrant of the nipple is located in the lower left corner of the image.

to be detected well above the cardiac rate. Previous systems achieving high sampling rates have utilized a small number of discrete modulation frequencies and wavelengths,[14,21] whereas the dDOS system sweeps a range of hundreds of modulation frequencies and utilizes six discrete wavelengths.

The dDOS system performance is comparable to previous systems. For example, Pham et al. reported an accuracy of $\pm 5\%$ and $\pm 3\%$ for μ_a and μ_s', respectively, whereas the dDOS system had an accuracy of $\pm 5.3\%$ and $\pm 5.5\%$ for the same parameters. The dDOS design has similarities to that of the modular digital FD diffuse optical monitor developed by Durduran et al., which utilized digital signal synthesis and a dual-channel ACD to sample and downconvert the signal from three laser wavelengths at a single modulation frequency;[21] however, our design differs in that we use six multiplexed laser wavelengths modulated at hundreds of discrete frequencies in the RF range. Zimmerman et al. recently developed a FD NIR high speed imaging system that utilized two wavelengths, two modulation frequencies, and an array of detectors; with this system, a measurement rate of 90 Hz was achieved, compared to the 97-Hz measurement rate achieved in the dDOS system with six wavelengths and a sweep of modulation frequencies.[14]

In the future, the portability of the system can be further improved by implementing miniaturized fiber-coupled laser diodes and miniaturized current driver modules that can be housed in a portable device enclosure. This will help to more easily measure patients in a clinical setting for a range of applications, such as chemotherapy monitoring or rapid hemodynamic analysis. The speed of the system also opens the possibility of monitoring rapid physiological changes at the cardiac rate, which may be useful in monitoring hemodynamics related to conditions, such as peripheral artery disease.

6 Conclusions

We have developed an inexpensive clinical FD-DOS platform based on DDSs and ADCs implemented on custom hardware-integrated PCBs. The system has high stability and accuracy in phantom measurements and is capable of detecting rapid physiological fluctuations above the cardiac rate using six wavelengths and a sweep of modulation frequencies. The dDOS

system may improve access to patients while helping to open new areas of investigation.

Disclosures

The authors have no conflicts of interest.

Acknowledgments

We would like to thank Dr. Eric Hazen and the Boston University Electronics Design Facility for their ongoing support with hardware and firmware development. The authors gratefully acknowledge funding from the American Cancer Society (Grant No. RSG-14-014-01-CCE) and the Department of Defense (Award No. W81XWH-15-1-0070).

References

1. B. J. Tromberg et al., "Non-invasive measurements of breast tissue optical properties using frequency-domain photon migration," *Philos. Trans. R. Soc. Lond. B. Biol. Sci.* **352**, 661–668 (1997).
2. B. J. Tromberg et al., "Optical property measurements in turbid media using frequency domain photon migration," *Proc. SPIE* **1525**, 52–58 (1991).
3. T. O. McBride et al., "A parallel-detection frequency-domain near-infrared tomography system for hemoglobin imaging of the breast in vivo," *Rev. Sci. Instrum.* **72**, 1817–1824 (2001).
4. J. P. Culver et al., "Three-dimensional diffuse optical tomography in the parallel plane transmission geometry: evaluation of a hybrid frequency domain/continuous wave clinical system for breast imaging," *Med. Phys.* **30**, 235–247 (2003).
5. T. H. Pham et al., "Broad bandwidth frequency domain instrument for quantitative tissue optical spectroscopy," *Rev. Sci. Instrum.* **71**, 2500–2513 (2000).
6. U. J. Netz, J. Beuthan, and A. H. Hielscher, "Multipixel system for gigahertz frequency-domain optical imaging of finger joints," *Rev. Sci. Instrum.* **79**, 034301 (2008).
7. Y. S. Yang et al., "Low-cost frequency-domain photon migration instrument for tissue spectroscopy, oximetry, and imaging," *Opt. Eng.* **36**, 1021–1569 (1997).
8. G. Yu et al., "Frequency-domain multiplexing system for in vivo diffuse light measurements of rapid cerebral hemodynamics," *Appl. Opt.* **42**, 2931–2939 (2003).
9. Y. Zhao et al., "Portable, parallel 9-wavelength near-infrared spectral tomography (NIRST) system for efficient characterization of breast cancer within the clinical oncology infusion suite," *Biomed. Opt. Express* **7**, 2186–2201 (2016).
10. B. Pogue et al., "Instrumentation and design of a frequency-domain diffuse optical tomography imager for breast cancer detection," *Opt. Express* **1**, 391–403 (1997).
11. S. J. Madsen et al., "Keywords: frequency-domain photon migration, optical properties, diode laser, network analyzer," *Proc. SPIE* **2389**, 257–263 (1995).
12. K.-S. No et al., "Design and testing of a miniature broadband frequency domain photon migration instrument," *J. Biomed. Opt.* **13**, 050509 (2009).
13. T. D. O'Sullivan et al., "Diffuse optical imaging using spatially and temporally modulated light," *J. Biomed. Opt.* **17**, 071311 (2012).
14. B. B. Zimmermann et al., "Frequency domain near-infrared multiwavelength imager design using high-speed, direct analog-to-digital conversion," *J. Biomed. Opt.* **21**, 016010 (2016).
15. J. Jung, R. Istfan, and D. Roblyer, "Note: a simple broad bandwidth undersampling frequency-domain digital diffuse optical spectroscopy system," *Rev. Sci. Instrum.* **85**, 076108 (2014).
16. D. Roblyer et al., "Feasibility of direct digital sampling for diffuse optical frequency domain spectroscopy in tissue," *Meas. Sci. Technol.* **24**, 045501 (2013).
17. J. Jung, R. Istfan, and D. Roblyer, "Note: a simple broad bandwidth undersampling frequency-domain digital diffuse optical spectroscopy system," *Rev. Sci. Instrum.* **85**, 076108 (2014).
18. W. G. Zijlstra and A. Buursma, "Spectrophotometry of hemoglobin: absorption spectra of bovine oxyhemoglobin, deoxyhemoglobin, carboxyhemoglobin, and methemoglobin," *Comput. Biochem. Physiol.* **118**, 743–749 (1997).
19. J. M. Bland and D. G. Altman, "Statistical methods for assessing agreement between two methods of clinical measurement," *Int. J. Nurs. Stud.* **47**, 931–936 (2010).
20. N. Shah et al., "Spatial variations in optical and physiological properties," *J. Biomed. Opt.* **9**, 534–540 (2004).
21. U. M. Weigel et al., "A new, modular frequency domain diffuse optical monitor in the digital domain," in *Digital Holography and Three-Dimensional Imaging*, Optical Society of America (2012).
22. J. Yong, A. Foo, and C. S. Lim, "Pulse transit time based on piezoelectric," *J. Clin. Monit. Comput.* **20**, 185–192 (2006).
23. W. Lee et al., "Systolic time intervals derived from electrocardiographic gated intra- renal artery Doppler waveform associated with left ventricular systolic function," *Sci. Rep.* **6**, 29293 (2016).
24. M. Vyas et al., "Augmentation index and central aortic stiffness in middle-aged to elderly individuals," *Am. J. Hypertens.* **20**, 642–647 (2007).
25. D. Roblyer et al., "Optical imaging of breast cancer oxyhemoglobin flare correlates with neoadjuvant chemotherapy response one day after starting treatment," *Proc. Natl. Acad. Sci. U. S. A.* **108**, 14626–14631 (2011).

Biographies for the authors are not available.

Journal of Biomedical Optics

BiomedicalOptics.SPIEDigitalLibrary.org

High-speed spatial frequency domain imaging with temporally modulated light

Matthew B. Applegate
Darren Roblyer

SPIE.

Matthew B. Applegate, Darren Roblyer, "High-speed spatial frequency domain imaging with temporally modulated light," *J. Biomed. Opt.* **22**(7), 076019 (2017), doi: 10.1117/1.JBO.22.7.076019.

Journal of Biomedical Optics 22(7), 076019 (July 2017)

High-speed spatial frequency domain imaging with temporally modulated light

Matthew B. Applegate and Darren Roblyer*
Boston University, Department of Biomedical Engineering, Boston, Massachusetts, United States

Abstract. Spatial frequency domain imaging (SFDI) is a wide-field diffuse optical technique used to obtain optical properties and chromophore concentrations in highly scattering media, such as biological tissue. Here, we present a method for rapidly acquiring multispectral SFDI data by modulating each illumination wavelength at a different temporal frequency. In the remitted signal, each wavelength is temporally demodulated and processed using conventional SFDI techniques. We demonstrate a proof-of-concept system capable of acquiring wide-field maps (2048×1536 pixels, 8.5×6.4 cm) of optical properties at three wavelengths in under 2.5 s. Data acquired by this method show a good agreement with a commercial SFDI imaging system (with an average error of 13% in absorption and 8% in scattering). Additionally, we show that this strategy is insensitive to ambient lighting conditions, making it more practical for clinical translation. In the future, this technique could be expanded to tens or hundreds of wavelengths without increasing acquisition time. [DOI: 10.1117/1.JBO.22.7.076019]

Keywords: diffuse optics; wide-field imaging; spatial frequency domain imaging.

Paper 170345R received May 27, 2017; accepted for publication Jul. 14, 2017; published online Jul. 31, 2017.

1 Introduction

At near-infrared wavelengths, biological tissue is highly scattering, making high-resolution images of tissue difficult at depths greater than about 1 mm.[1] However, multiply scattered photons carry information about the absorption coefficient (μ_a) and the reduced scattering coefficient (μ_s'), which can reveal the function and structure of the sample. From these optical properties, the concentration of biologically relevant chromophores, such as oxy- and deoxyhemoglobin, lipid, and water, can be deduced. Knowledge of these chromophore concentrations provides a wealth of information about the composition and metabolic activity of tissue, which has proven useful in oncology,[2,3] small animal imaging,[4] exercise physiology,[5] and imaging the brain.[6,7] Most diffuse optics techniques use point-by-point scanning to build up a map of tissue optical properties, but this strategy limits the area and resolution with which tissue can be probed in a clinically relevant period of time.[8] Efforts to increase speed and resolution of point-by-point systems typically involve increasing the number of sources and detectors (often into the hundreds), resulting in devices that are expensive, bulky, and specific to particular anatomical sites.[9,10] Recently, a new technique called spatial frequency domain imaging (SFDI) has been shown to provide wide-field determinations of optical properties of scattering media without point-by-point scanning.[11,12] SFDI involves the illumination of tissue with spatially modulated light and the recording of diffuse reflectance remitted by the tissue using a camera. The response of the tissue in the spatial frequency domain can be related to the spatial domain by an inverse Fourier transform, resulting in 2-D maps of the diffuse reflectance. The resulting reflectance maps can then be used to determine optical properties at each pixel of the image.

*Address all correspondence to: Darren Roblyer, E-mail: roblyer@bu.edu

The first described SFDI processing technique used a minimum of six image acquisitions per wavelength. At each of at least two spatial frequencies, images of the sample were acquired with three spatially offset phases, which were demodulated to obtain the envelope of the diffusely reflected light.[12] This envelope contains information about the structure and composition of the tissue under investigation. During demodulation, DC background illumination is subtracted from the resulting images, rendering this technique theoretically insensitive to ambient light so long as it remains constant during the acquisition. However, the collection of multiple images, as well as the time needed to switch between wavelengths, results in acquisitions times that typically stretch into the tens of seconds. Recently, more advanced demodulation techniques have reduced the number of images needed to two per wavelength,[13] or one per wavelength in a technique termed "single-shot optical properties" (SSOP).[14,15] This method exploits the fact that sinusoidal patterns of light contain at least two spatial frequencies: the DC offset with a spatial frequency of 0 and the AC component at the projected spatial frequency. Low-pass filtering of the image effectively separates out the DC component, while the envelope of the higher frequency component can be computed using a Hilbert transform, or other single-sideband demodulation technique.[16] The single-shot processing method reduces the number of images that need to be acquired at each wavelength from six to one, but still requires that each wavelength be collected sequentially. Furthermore, this technique is more sensitive to changes in ambient light than the original method, posing a challenge for fast-paced clinical environments, where lighting conditions may be constantly changing.

Here, we present a new SFDI acquisition method that enables the rapid collection of optical properties simultaneously from a large number of wavelengths while being insensitive to ambient light. The method borrows from a technique previously used to

enhance hyperspectral fluorescence imaging speed by modulating each excitation wavelength at different temporal rates.[17] In this study, we use three wavelengths of light that are temporally modulated at different frequencies and then used to project a single sinusoidal illumination pattern. We call this method "temporally modulated SFDI" (TM-SFDI). By collecting a sequence of images of the sample while it is illuminated with time-varying light, each pixel of the video can be temporally demodulated by determining the strength of the reflected signal at each modulation frequency. The result of temporal demodulation is a single spatially modulated image at each wavelength, which can then be processed using the SSOP method. Because this technique is only sensitive to light modulated at a specific frequency, it automatically rejects ambient light, unlike conventional single-shot processing. Additionally, because there is no need to switch between wavelengths or projection patterns, acquisition speeds are only limited by the frame rate of the camera and the number of video frames needed for successful temporal demodulation. In Sec. 2, we will describe how the TM-SFDI system was realized; Sec. 3 demonstrates that it is capable of accurately determining optical properties, is insensitive to ambient light, and can be used to image complex samples.

2 Materials and Methods

2.1 *Hardware*

For this proof-of-concept system, three wavelengths of light were used: 519, 652, and 740 nm. One high-power LED per wavelength (Cree XLamp, Cree, Inc. Durham, North Carolina) was driven at 700 mA (652 and 740 nm) or 1000 mA (519 nm) with independent constant current sources. Light from the LEDs was modulated in time using a pulse-width modulation sequence controlled by a microcontroller (Arduino UNO). Modulation frequencies were set at 5.21, 8.68, and 12.15 Hz, each of which falls into a single bin of a 32 point discrete Fourier transform when a sampling period of 18 ms (55.6 frames/s) is used. Frequencies occupying a single bin were important for reducing cross-talk between wavelengths. These frequencies were also chosen to avoid harmonic content from lower frequencies influencing higher frequency modulation. Light from the LEDs was roughly collimated by a lens over each emitter and sent through a transparency printed with a sine wave pattern using a laser jet printer [Fig. 1(a)]. The spatiotemporally modulated light was directed onto a sample, and the reflected light was recorded by a 16 bit scientific CCD camera (Zyla 4.2, Andor, Inc.) with an 8.5×6.4 cm field-of-view (FoV). Crossed polarizers were used to minimize the effect of specular reflection. Modulation and acquisition timings were controlled by a custom Arduino program.

2.2 *Processing*

Videos of temporally modulated light reflected from the sample were acquired at 55.6 frames/s for 2.3 s (128 frames) for offline processing. A Fourier transform in time of each pixel of the image was performed to separate the wavelengths. The amplitude of the spectrum at each modulation frequency corresponded to the intensity of the light reflected by that specific wavelength at that specific spatial location [Fig. 1(b)]. Recording the strength of the peaks at each pixel effectively separates each wavelength, while simultaneously rejecting background light (Fig. 2). Once an image of each wavelength was extracted, the images were rotated to ensure that the stripes were parallel to the top and bottom of the frame, and the optical properties were determined by previously published techniques.[14] Briefly, each image was split into a DC and AC component by taking a spatial Fourier transform of each line of the image and filtering in the spatial frequency domain. The DC image was generated by removing a band of frequencies surrounding the projected AC frequency, leaving the high and low frequency content intact. The inverse Fourier transform of this spectrum was used to determine the diffuse reflectance of the sample under planar illumination. The AC image was

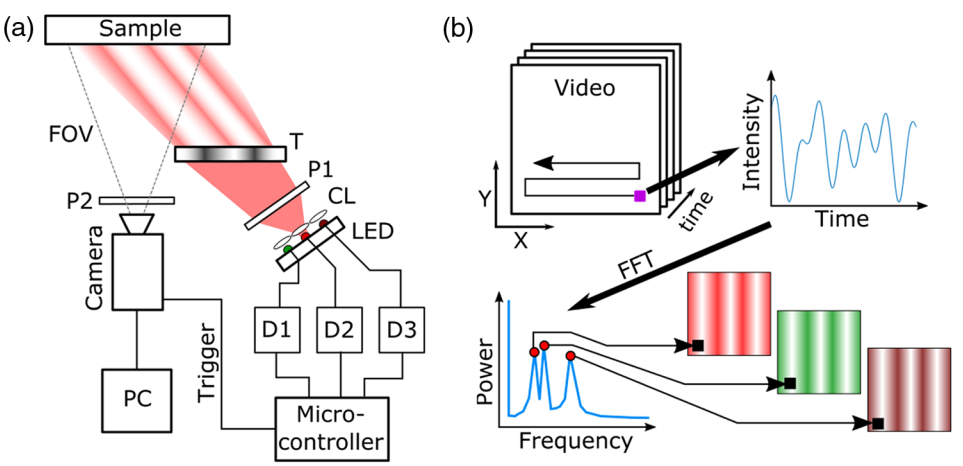

Fig. 1 (a) System diagram. Three LEDs were driven by independent constant current sources (D1, D2, D3) and were temporally modulated by a microcontroller. The light was roughly collimated by three lenses (CL) and polarized (P1) before passing through a patterned transparency (T). Before being imaged by the camera, reflected light passed through a second polarizer (P2) set at 90 deg to P1 to reject specular reflection. Camera FoV is indicated by dashed lines. (b) Schematic of data processing. A video was captured from the camera and the variation of each pixel in time was plotted. An FFT of this time series was taken and the strength of the signal at the frequencies corresponding to the modulation of the LEDs was used to build up a 2-D image for each wavelength. These temporally demodulated images were then processed using the SSOP technique as in Ref. 14.

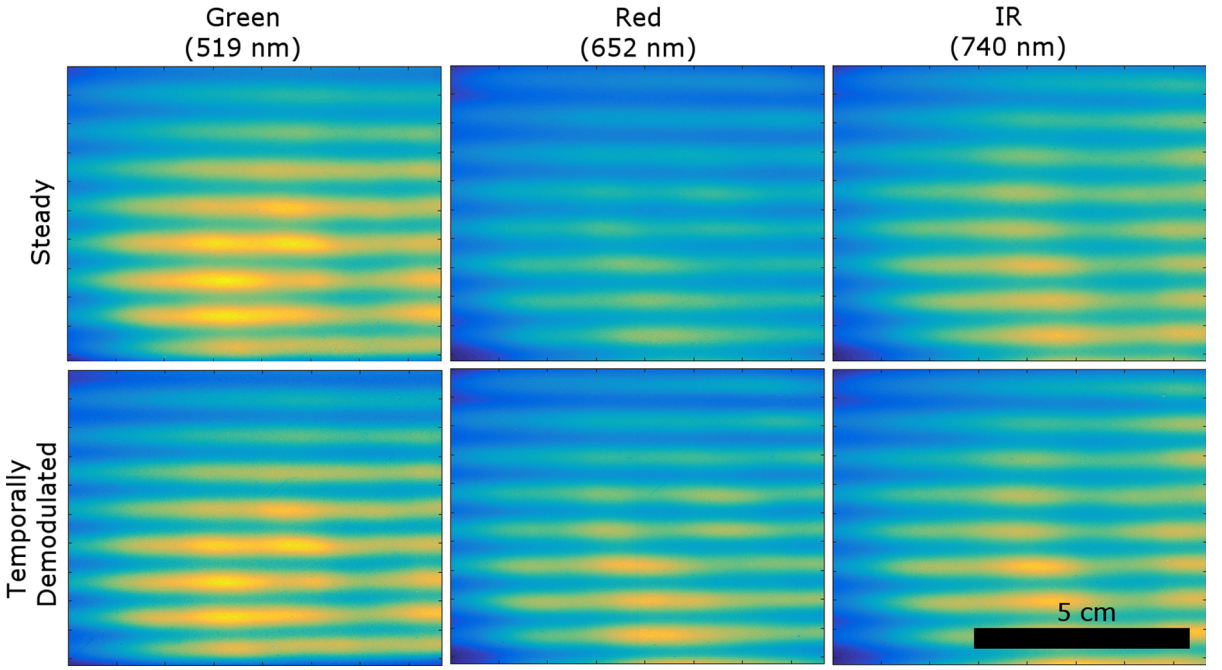

Fig. 2 Comparison of normalized images taken of the spatial pattern when the LEDs were individually illuminated without temporal modulation (top row) versus temporally demodulated images of each wavelength using the TM-SFDI system (bottom row). The images closely match, showing the ability of temporal demodulation to separate different wavelengths. The scale bar applies to all images.

obtained via Hilbert transform followed by inverse Fourier transform of the high frequency content. The demodulated AC and DC images were compared with a reference standard to obtain the calibrated reflectance of each pixel in the image. Optical properties were calculated by interpolating a look-up table relating calibrated reflectance values to optical properties, which was generated by scaling of a single Monte Carlo simulation.[12,18]

2.3 *Accuracy and Drift*

To test the accuracy of the TM-SFDI system, a set of 13 tissue mimicking phantoms with varying optical properties were imaged three times over 3 days with a commercial SFDI system (OxImager RS, Modulated Imaging, Inc.) at wavelengths of 526, 659, and 729 nm to establish the "gold standard" measurements of the phantom optical properties. The same set of phantoms was also imaged three times over 3 days with the TM-SFDI system at wavelengths of 519, 652, and 740 nm. Both systems used measurements of a reference standard with known optical properties for instrument response calibration. To account for variability in the TM-SFDI system, the reference standard was imaged five times per day and the temporally demodulated images were averaged together before being used to calculate μ_a and μ_s' at each wavelength. Optical properties of the phantoms from both the commercial system and the TM-SFDI system were calculated using the same SSOP algorithm and compared against each other. Because the same wavelengths were not available for both systems, a correction factor was implemented to estimate the optical properties calculated by the commercial system at the wavelengths used in the TM-SFDI system. To construct the correction factor for μ_a, the absorption spectrum of nigrosin, the chromophore used to make the tissue mimicking phantoms, was measured using a spectrophotometer. The correction factor for absorption was defined as $\mu_a(\lambda_{TM}) = \frac{\mu_a(\lambda_{Com})\epsilon(\lambda_{TM})}{\epsilon(\lambda_{Com})}$, where $\mu_a(\lambda_{TM})$ is the estimated absorption coefficient at the TM-SFDI wavelength λ_{TM}, $\mu_a(\lambda_{Com})$ is the measured absorption coefficient at the wavelength of the commercial system (λ_{Com}), and $\epsilon(\lambda)$ is the extinction coefficient of nigrosin at the wavelength λ measured with the spectrophotometer. To estimate how μ_s' changes with wavelength, we assumed a Rayleigh scattering ($\mu_s' \propto \lambda^{-4}$) relationship and defined the correction factor as $\mu_s'(\lambda_{TM}) = \frac{\mu_s'(\lambda_{Com})\lambda_{Com}^{-4}}{\lambda_{TM}^{-4}}$, where $\mu_s'(\lambda_{Com})$ is the reduced scattering coefficient calculated by the commercial system at λ_{Com}. Rayleigh scattering was assumed because scattering in the phantoms is controlled by altering the concentration of titanium dioxide nanoparticles, the diameters of which are much smaller than the wavelengths of light used. The maximum change in optical properties using these correction factors was slightly over 5%. Each TM-SFDI scan consisted of 128 2048×1536 pixel images, with an FoV of 8.5×6.4 cm. To improve the signal-to-noise ratio, the temporally demodulated images were downsampled using 2×2 averaging.

To assess the stability of the TM-SFDI system, a single tissue mimicking phantom was scanned every 10 min for 2 h following a 30-min warm up period, and the variations in calibrated reflectance and optical properties at each wavelength over that time were calculated based on comparison with a reference standard imaged at the start and end of the drift test. Each scan consisted of 128 images.

2.4 *Effect of Ambient Light*

To test the effect of ambient light on TM-SFDI, a calibration phantom was imaged in complete darkness. TM-SFDI videos were then acquired at various levels of ambient light controlled

by changing the distance between the bulb of a standard desk lamp and the sample. Images of a single wavelength not modulated in time were also acquired to compare the TM-SFDI technique with the SSOP method.

3 Results and Discussion

3.1 *Accuracy*

We found that there was a good agreement in optical property extractions between the gold standard commercial instrument and the proof-of-concept TM-SFDI system (Fig. 3). The average error in absorption between the TM-SFDI and the gold standard was 13%. The TM-SFDI system was more accurate at extracting reduced scattering, with an average error of 8% compared with the gold standard. The absorption measurements were biased, consistently underestimating the actual absorption coefficient by an average of 0.003 mm^{-1}, while the scattering measurements were biased in the other direction, overestimating μ_s' by an average of 0.088 mm^{-1}.

In addition to homogeneous phantoms, a more complex tissue simulating phantom was imaged. The sample was a 3-D printed block of acrylonitrile butadiene styrene that featured a network of vascular like channels filled with a highly absorbing acrylic copolymer (P400SR, Stratasis, Inc.). The complex phantom was imaged with the TM-SFDI system, and a good correlation between the printed channel and the absorption map was noted (Fig. 4).

3.2 *Drift*

The drift of the TM-SFDI system was tested by allowing the system to warm up for 30 min and then repeatedly measuring the same phantom every 10 min for 2 h. The average changes in calibrated reflectance over this time period were less than 3% for the AC and DC components. However, these errors translated into a relatively large average variation in μ_a of 13% about the mean. The average variation in μ_s' was 1%. There was no systematic rise or fall to the change but rather a random variation about the mean. To determine the source of the drift, we tested each LED individually with DC illumination and no temporal modulation and found a variation of 1% to 3% of output intensity over time. Though relatively small, this variation would also change the calibrated reflectance by the same 1% to 3%, which maps to a greater than 10% change in μ_a. The observed variation in optical properties is likely due to instability of the LEDs and driver electronics, which were both consumer grade. We expect that upgrading these components and implementing temperature control would reduce the variability in measured optical properties.

3.3 *Effect of Ambient Light*

We found that the TM-SFDI system was almost entirely insensitive to the ambient light level. In Fig. 5, the calibrated reflectance for planar illumination is shown for SSOP (blue) and TM-SFDI (red) along with linear fits to the data at a variety of ambient light levels. The slope of the linear fit of the TM-SFDI DC reflectance was not significantly different from zero ($p = 0.5$) using a two sided t-test, indicating that there was no relationship between ambient light level and calibrated reflectance. The change in calibrated reflectance using SSOP would result in extremely large errors in optical properties as ambient illumination changed. Future instruments using TM-SFDI will need to avoid frequencies near the AC power supply (typically 50 or 60 Hz) to avoid contamination from the flickering of room lights.

3.4 *Discussion*

The TM-SFDI system presented here allows for the rapid acquisition of diffuse optical images. At 56 frames/s and a typical video length of 128 frames, we were able to capture spectroscopic images of optical properties at three wavelengths in 2.3 s. The number of simultaneous wavelengths that can be collected is limited by the number of video frames acquired. The

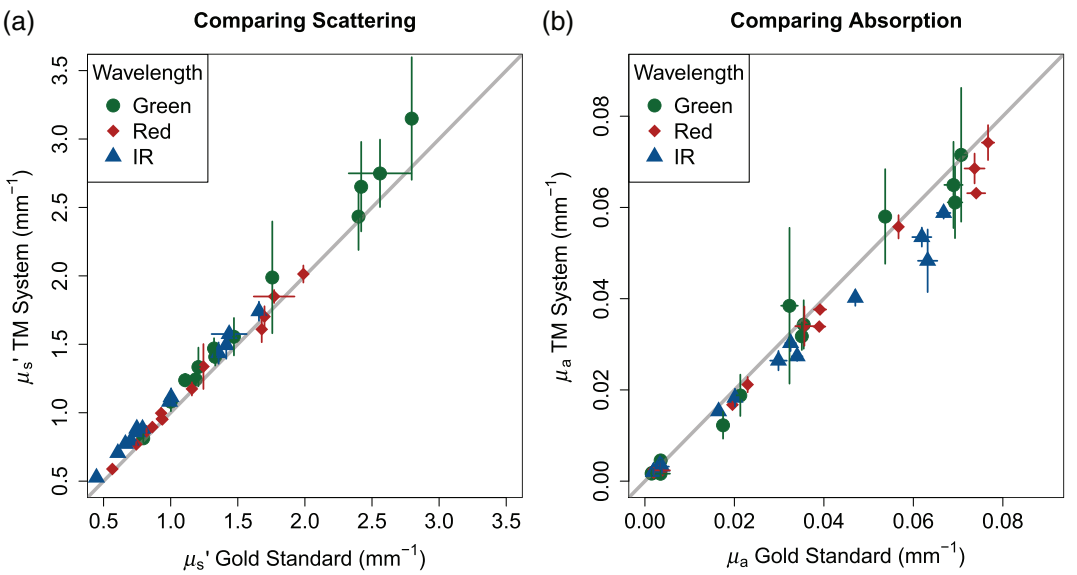

Fig. 3 Comparison of TM-SFDI with gold standard in terms of (a) scattering and (b) absorption. The identity line is shown in gray. Error bars indicate ±1 standard deviation of the average measured optical property across the 3 days. Acquisition time was 2.3 s for the TM system versus ~30 s for the gold standard device.

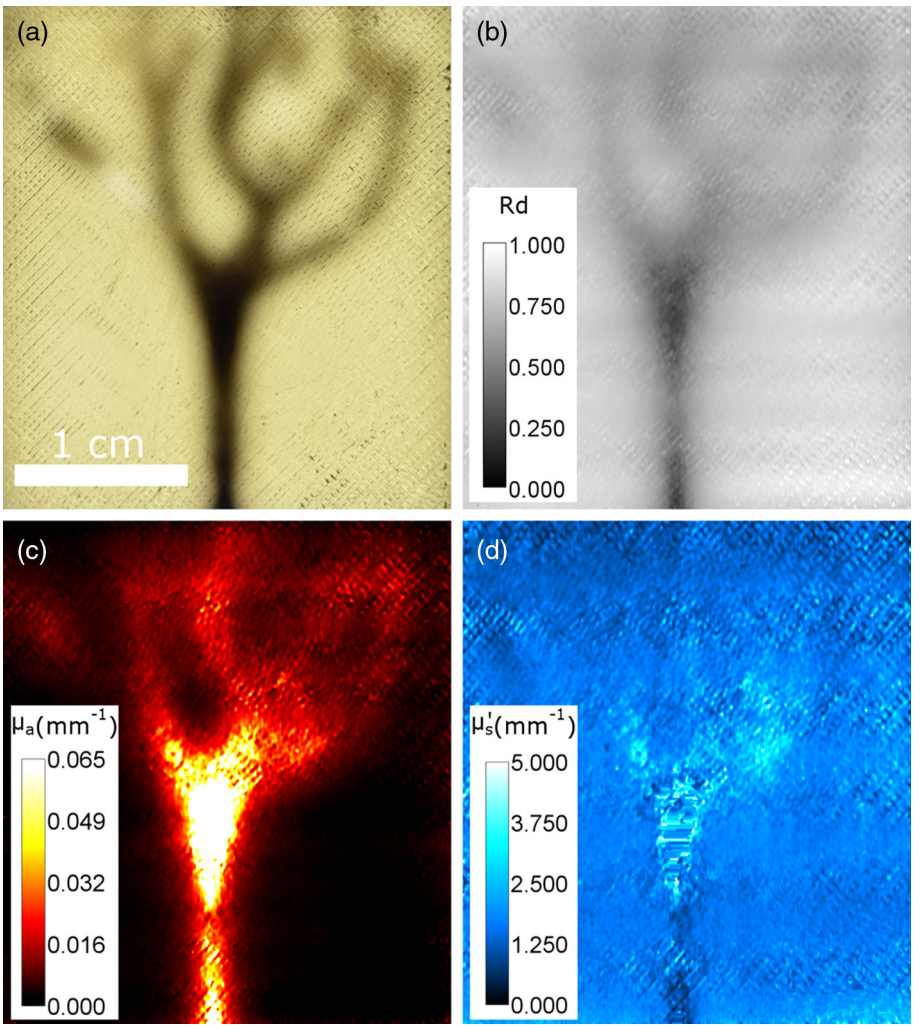

Fig. 4 (a) Photograph of the 3-D printed phantom with vessel-like inclusions under strong back illumination. (b) Temporally and spatially demodulated image of calibrated DC reflectance at 652 nm. (c) Map of the absorption coefficient and (d) map of the reduced scattering coefficient of the sample (d) at 652 nm. Scale bar applies to all images. Median filtering was used on panels (c) and (d) to remove artifacts.

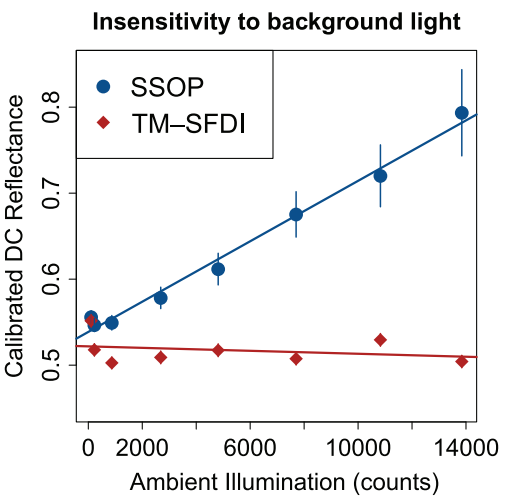

Fig. 5 Temporally modulated (blue) SFDI compared with single shot SFDI (red) under varying levels of ambient light. TM-SFDI is largely insensitive to the ambient light level while SSOP is highly sensitive. Error bars represent ±1 standard deviation of the pixels in the image.

maximum number of wavelengths that can be unambiguously demodulated is no more than one per FFT bin (excluding DC). This means that a 128 frame scan could theoretically support 63 wavelengths, while a 256 frame scan could support 127, although practically, this number of wavelengths may be reduced due to spectral leakage. We experimented with using fewer video frames (64, 32, 16, etc.) and found an increased scan-to-scan variability. Using 64 images, there were only modestly higher errors (10% in scattering and 24% in absorption), meaning acquisition speeds of around 1 s with reasonable errors are possible. Since the maximum frame rate of the camera increases when fewer CCD lines need to be read, using a smaller FoV could also increase acquisition speed. For an image of 512×512 pixels, it would be possible to increase the frame rate from 55.6 to 80 fps, resulting in a minimum acquisition time of 800 ms for up to 16 wavelengths.

Recent work has utilized a similar temporal modulation of excitation wavelengths for single pixel SFDI.[19] Despite advantages in simplicity of hardware, cost, and bandwidth, single pixel imaging scales poorly with resolution, requiring the projection of over 31,000 patterns for each spatial frequency and

phase to acquire an image with a comparable number of pixels used in this study. For example, Torabzadeh et al.[19] used single-pixel SFDI to acquire 400 samples in 80 ms, meaning a single high resolution image could be collected every 6.2 s. While a large number of pixels is not strictly necessary for low-resolution diffuse imaging, it allows for pixel binning to reduce the overall noise level. Greater numbers of pixels would also allow for the possibility of imaging larger FoVs without impacting resolution.

The TM-SFDI system has several limitations worth noting. The first is variability in μ_a extractions. The errors in absorption are likely due to the fact that, at the chosen spatial frequencies, small changes in reflectance map to large changes in μ_a, meaning that the effects of noise and LED instability are amplified.[4] It is likely that temperature variations of the LEDs and driver circuit led to instability of the LED output and resulted in uncertainty in the absorption estimates. We also found that the estimates for optical properties were biased with the absorption being underestimated and the scattering overestimated. We believe both biases are due to broadband noise contaminating the images, resulting in small, systematic errors in diffuse reflectance as well as nonlinearities in system response, which are not accounted for in the calibration step and result in increased errors for samples with optical properties that differ significantly from the calibration phantom. It is likely that improvements in the signal-to-noise ratio and careful choice of calibration phantom will help resolve this issue. Second, the acquisition time of 1 to 2 is relatively long compared with the SSOP method, and the sample must be held motionless for that entire time to achieve a clear image of the resulting optical properties. This could potentially be solved by adding an image registration step to align the frames of the video prior to processing. Third, although scans can be performed relatively quickly, processing of the data requires significant computational resources. Each scan requires over 300,000 FFTs to be performed as well as searching a nonlinear look-up-table for each pixel at each wavelength. On a relatively modern desktop computer (Intel i7-6700, 16 GB RAM), the time to process each scan was about 80 s. However, much of the processing is parallelizable and could likely be vastly sped up by offloading to a graphics processing unit.

4 Conclusion

In conclusion, we have constructed a high-speed SFDI system that enables the acquisition of spectrally resolved optical properties without needing to switch between illumination patterns or wavelengths. Currently, the system operates at ~750 ms/wavelength, but, since acquisition time does not scale with the number of wavelengths used, this could be increased to ~50 ms/wavelength by adding additional illumination wavelengths. By mapping the spectral components of light into the time domain, this system eliminates the need to acquire each wavelength sequentially. Importantly, the temporal modulation of light also makes this system insensitive to background illumination, making it a practical technique for translation into the clinic, where light levels vary widely and cannot easily be controlled. Future work will investigate increasing the stability of the LEDs, increasing the number of modulated wavelengths using dispersed supercontinuum light in conjunction with a linear spatial light modulator, testing the TM-SFDI on a variety of biological samples, and including single-shot height correction for more accurate imaging of 3-D samples.[15]

Disclosures

The authors have no conflicts of interest to disclose.

Acknowledgments

The authors gratefully acknowledge funding from the U.S. Department of Defense (DoD) (Award No. W81XWH-15-1-0070).

References

1. W. R. Zipfel et al., "Live tissue intrinsic emission microscopy using multiphoton-excited native fluorescence and second harmonic generation," *Proc. Natl. Acad. Sci. U. S. A.* **100**, 7075–7080 (2003).
2. D. Roblyer et al., "Optical imaging of breast cancer oxyhemoglobin flare correlates with neoadjuvant chemotherapy response one day after starting treatment," *Proc. Natl. Acad. Sci. U. S. A.* **108**, 14626–14631 (2011).
3. P. G. Anderson et al., "Broadband optical mammography: chromophore concentration and hemoglobin saturation contrast in breast cancer," *PLoS One* **10**(3), e0117322 (2015).
4. S. Tabassum et al., "Feasibility of spatial frequency domain imaging (SFDI) for optically characterizing a preclinical oncology model," *Biomed. Opt. Express* **7**(10), 4154–4170 (2016).
5. T. Hamaoka et al., "The use of muscle near-infrared spectroscopy in sport, health and medical sciences: recent developments," *Philos. Trans. R. Soc. A* **369**(1955), 4591–4604 (2011).
6. A. V. Medvedev et al., ""Seeing" electroencephalogram through the skull: imaging prefrontal cortex with fast optical signal," *J. Biomed. Opt.* **15**(6), 061702 (2010).
7. D. A. Boas et al., "The accuracy of near infrared spectroscopy and imaging during focal changes in cerebral hemodynamics," *Neuroimage* **13**(1), 76–90 (2001).
8. F. Bevilacqua et al., "Broadband absorption spectroscopy in turbid media by combined frequency-domain and steady-state methods," *Appl. Opt.* **39**, 6498–6507 (2000).
9. C. Li et al., "Multispectral breast imaging using a ten-wavelength, 64×64 source/detector channels silicon photodiode-based diffuse optical tomography system," *Med. Phys.* **33**(3), 627–636 (2006).
10. A. T. Eggebrecht et al., "Mapping distributed brain function and networks with diffuse optical tomography.," *Nat. photonics* **8**(6), 448–454 (2014).
11. N. Dögnitz and G. Wagnières, "Determination of tissue optical properties by steady-state spatial frequency-domain reflectometry," *Lasers Med. Sci.* **13**(1), 55–65 (1998).
12. D. J. Cuccia et al., "Quantitation and mapping of tissue optical properties using modulated imaging," *J. Biomed. Opt.* **14**(2), 024012 (2009).
13. K. P. Nadeau, A. J. Durkin, and B. J. Tromberg, "Advanced demodulation technique for the extraction of tissue optical properties and structural orientation contrast in the spatial frequency domain," *J. Biomed. Opt.* **19**(5), 056013 (2014).
14. J. Vervandier and S. Gioux, "Single snapshot imaging of optical properties," *Biomed. Opt. Express* **4**(12), 2938–2944 (2013).
15. M. van de Giessen, J. P. Angelo, and S. Gioux, "Real-time, profile-corrected single snapshot imaging of optical properties," *Biomed. Opt. Express* **6**(10), 4051 (2015).
16. S. L. Hahn, *Hilbert Transforms in Signal Processing*, Vol. **2**, Artech House, Boston (1996).
17. S. R. Domingue, D. G. Winters, and R. A. Bartels, "Hyperspectral imaging via labeled excitation light and background-free absorption spectroscopy," *Optica* **2**(11), 929 (2015).
18. M. Martinelli et al., "Analysis of single Monte Carlo methods for prediction of reflectance from turbid media," *Opt. Express* **19**(20), 19627 (2011).
19. M. Torabzadeh et al., "Compressed single pixel imaging in the spatial frequency domain," *J. Biomed. Opt.* **22**(3), 030501 (2017).

Matthew B. Applegate is a postdoctoral researcher in the Department of Biomedical Engineering at Boston University. He received his BS in electrical engineering from Cornell University in

2009 and his PhD in biomedical engineering from Tufts University in 2016. His current research interests are focused on developing new, clinically translatable optical techniques using diffuse optics, OCT, and nonlinear optics.

Darren Roblyer is an assistant professor in the Department of Biomedical Engineering at Boston University. After receiving his BS degree in biomedical engineering from Johns Hopkins University in 2004, he received his PhD as a HHMI Med-Into-Grad Fellow in 2009 from the Bioengineering Department at Rice University, where he studied under Rebecca Richards-Kortum. Prior to starting his faculty position in 2012, he was a postdoctoral fellow at the Beckman Laser Institute studying under professor Bruce Tromberg.